Engineering nanostructured electrodes and fabrication of film electrodes for efficient lithium ion intercalation

Dawei Liu and Guozhong Cao*

Received 29th October 2009, Accepted 18th March 2010
DOI: 10.1039/b922656g

Lithium ion batteries have been one of the major power supplies for small electronic devices since the last century. However, with the rapid advancement of electronics and the increasing demand for clean sustainable energy, newer lithium ion batteries with higher energy density, higher power density, and better cyclic stability are needed. In addition, newer generations of lithium ion batteries must meet the requirements of low and easy fabrication cost and be free of toxic materials. There have been many novel approaches to gain high energy storage capacities and charge/discharge rates without sacrificing the battery cyclic life. Nanostructured electrodes are seemingly the most promising candidate for future lithium ion batteries. Modification of the electrode surface chemistry and the control of appropriate crystallinity are also reported to improve the electrode intercalation capabilities. The study of appropriately designed nanostructures, interfaces and crystallinity has also promoted and is accompanied with the development of thin film electrodes without the addition of binders and conductive carbon that are typically used in the fabrication of traditional lithium ion battery electrodes, simplifying the electrode fabrication process and enhancing electrode storage density. In this perspective, we summarize and discuss the efforts of fabricating nanostructures, modifying surface chemistry and manipulating crystallinity to achieve enhanced lithium ion intercalation capacities, rate capabilities and cyclic stability, as well as the direct fabrication of binderless film electrodes with desirable nano- and microstructures.

1. Introduction

1.1 Lithium ion battery as energy storage device background

Energy has been the central focus of human development since global industrialization. Fossil fuels have been and are still the major energy source with much improved energy conversion efficiency and significantly reduced environmental pollution as a result of combined technology advancement and the public awareness of the health and environmental challenges associated with fossil fuels. Although renewable or sustainable energy including solar, wind, and hydro-energy remains a negligible fraction of our total energy consumption today,[1,2] energy security and environmental concerns have spurred great technical and political interests in developing advanced technologies to improve the energy utilization efficiency including smart electrical grid[3,4] and light emitting materials and devices,[5,6] to reduce and recover the "waste" heat through developing smart building materials and structure,[7] and converting the waste heat to electricity using thermoelectrics,[8,9] and to harvest the clean and sustainable energy such as solar, wind and tidal energy.[10–12]

Advanced energy storage technologies for vehicle electrification and efficient use of renewable energy from the sun and wind are a critical part of renewable energy.[13,14] Several technologies are currently under intensive study.[15–17] Generating biofuels from biomass is one example of converting solar energy to chemical fuels.[18,19] Storing hydrogen in the liquid or solid forms near ambient conditions is another example.[20,21] However, effective utilization of variable and intermittent sources of renewable energy in meeting growing electricity demand requires much improved electrical energy storage technologies that are

Department of Materials Science and Engineering, University of Washington, Seattle, WA, USA 98195. E-mail: gzcao@u.washington.edu

Broader context

In the new century, clean and renewable energy storage devices have become the foci of both the building industry and research development. Lithium ion batteries, as one of the most promising battery technologies, have attracted much attention due to their fast boom of market share. However, the commercialized lithium ion battery has not been good enough to satiate the public need and theoretically there is much room for improvement. Research has thus been focused on developing electrode materials with high discharge capacity, large charge/discharge rate and long life cycles. To achieve these goals, a lot of effort has been devoted to fabricating structures that best facilitate the intercalation behavior of lithium ions. In this perspective, these efforts are summarized and reported.

economically viable to enable large scale market penetration for electric vehicles and renewable electricity storage. Capacitors and supercapacitors, also known as ultracapacitors, offer high specific power and long cyclic stability and life time, and thus are excellent choices for applications requiring a burst energy source; however, they suffer from low specific energy.[22,23] Batteries possess great specific energy, but suffer from low specific power and cyclic degradation.[24,25] Significant breakthroughs are needed for both supercapacitors and batteries to gain broad market penetration.

Batteries are more than a century old technology and have played critical roles in many technologies and today's mobile life. Although many types of batteries have been developed with much improved energy storage performance, the fundamental structure of a battery remains the same, consisting of an anode and a cathode with electrolyte sandwiched in between.[26] The advancement in battery technology has been relying on the development and use of different types of materials for electrodes and electrolytes and thus with different electrochemical reactions.[27,28] Fig. 1 compares different types of batteries;[29] lithium-ion batteries offer a balanced combination of high power and energy density, long cyclic life, and stability. The commercialization of lithium ion batteries has witnessed the soaring market share in the energy industry, especially in powering small electronic devices such as laptops and cellular phones.[30,31]

A lithium ion battery, just like other types of batteries, consists of three major components: an anode, a cathode, and the electrolyte between them, and works by converting chemical potential to electric energy through Faradaic reactions, which include heterogeneous charge transfer process occurring at the surface of an electrode.[32] Different from disposable or primary batteries, the lithium ion battery is a rechargeable or secondary battery, and the charging process involves the energy conversion from electric energy back to chemical potential.[33] In a typical secondary lithium ion battery, Faradaic reactions are accompanied with both mass and charge transfer through the electrodes as well as dimension change; therefore, the surface area and the transport distance critically determine the performance of the battery in question.[34] Chemical composition, crystal structure,

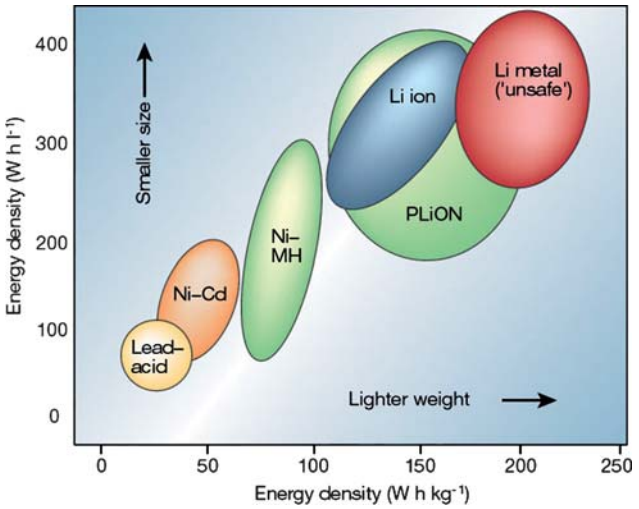

Fig. 1 Comparison of the different battery technologies in terms of volumetric and gravimetric energy density. It is clear that for a given energy storage, lithium ion batteries are lighter and smaller. In addition, the lithium ion batteries are more environmental benign.[29]

and microstructure will have significant impacts on the reaction rate and transfer processes as well as its cyclic stability.[29,35]

1.2 The performance of lithium ion intercalation electrodes

Energy storage density of a lithium-ion battery. Energy storage density of a lithium-ion battery, also known as specific energy when counted as per unit mass, is determined by (1) the lithium ion storage capacity, C, and (2) the cell voltage, V, which is the difference of electrochemical potentials of the anode and the cathode used in the battery in question and calculated using the following equation:

$$E = CV \quad (1)$$

Obviously, a high energy storage density can be achieved by choosing or developing anodic and cathodic materials with high

Dawei Liu

Mr. Dawei Liu is a PhD candidate under the supervision of Prof. Guozhong Cao in Department of Materials Science and Engineering at University of Washington, Seattle, WA. He has published five first-authored refereed papers and one book chapter. His specific research project is focused on nanostructured electrodes for efficient lithium ion intercalation.

Guozhong Cao

Dr Guozhong Cao is Boeing–Steiner Professor of Materials Science and Engineering at the University of Washington, Seattle, WA. He has published over 250 refereed papers, written and edited five books and monographs. His research has led to the creation of two spin-off companies on energy conversion and storage. His recent research is focused mainly on nanomaterials for solar cells, lithium ion batteries, supercapacitors, and hydrogen storage.

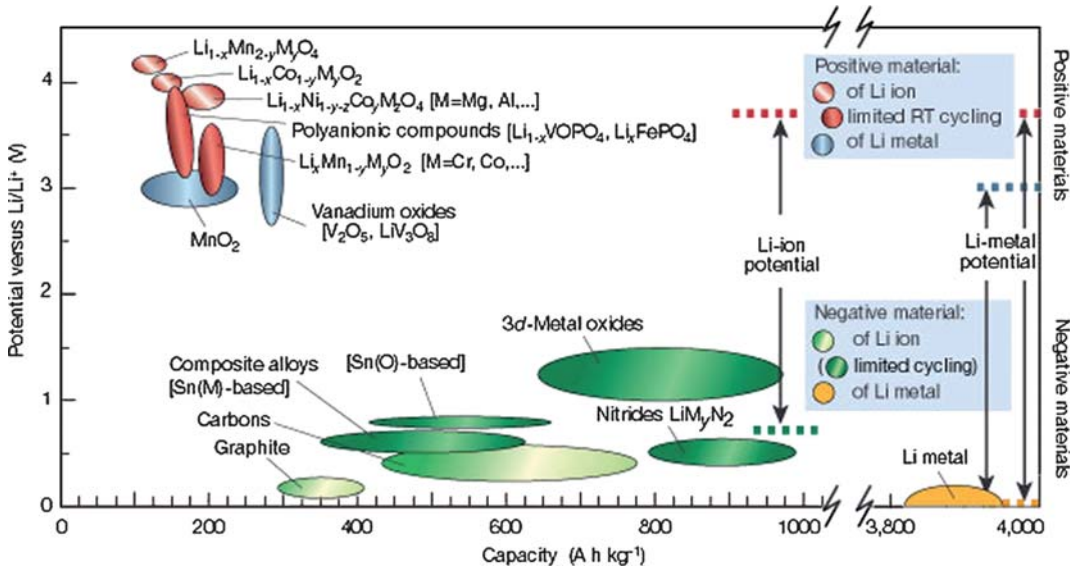

Fig. 2 Voltage *vs.* capacity for positive and negative electrode materials presently used for under serious consideration for the next generation of rechargeable Li-based cells.[29]

lithium-ion intercalation capacity with a large electrochemical potential difference. Although increasing the potential of cathodic materials and, thus increasing the cell voltage, with a given anode, is seemingly the most effective way to increase the energy storage density, the decomposition of electrolyte at the cathode surface becomes a problem.[34] Before finding suitable electrolytes stable at high cathode potential, the research is focused mostly on the development of electrodes with high lithium ion intercalation capacity. Fig. 2 summarizes the electrochemical potential and the typical lithium ion storage capacities of both anodic and cathodic materials.[29]

While the lithium ion intercalation capacity of anodes, *e.g.* Sn can stabilize well above 500 mA h g^{-1} even after a big capacity loss following the initial cycle,[36,37] the highest capacity of cathode materials is way below 500 mA h g^{-1}. As a result, the performance of the cathode is a bottleneck for the improvement of the whole battery system.[38,39] For example, the commercialized $LiCoO_2$ has a mere capacity of ~140 mA h g^{-1},[40] and its potential alternatives $LiMn_2O_4$ and $LiFePO_4$ have capacities of merely 150,[41] and 170 mA h g^{-1}, respectively.[42] The cathode compounds demand more research efforts for new lithium ion batteries with much enhanced energy storage density.

Rate capability. Rate capability is another parameter to evaluate an electrode performance. Unfortunately, the energy storage mechanism of lithium ion battery by an intercalation process leads to the poor rate capability caused by the low kinetics of the lithium ion and charge transfer process and diffusion inside the electrode. Conductive additives are commonly admixed with electroactive materials (intercalation compounds) to fabricate electrodes with improved electrical conductivity.[43,44]

Cyclic stability. One of the selling points of lithium ion batteries is the rechargeability which saves money and the environment. However, the lithium ion intercalation process induces a volume change of the electrode and thus a stress gradient between the surface and interior will be generated during the intercalation and de-intercalation process, which would inevitably lead to the loss of integrity of the electrodes and thus degrade long-term cyclic stability.

1.3 Solutions by constructing specially designed structures

The lithium ion intercalation/de-intercalation process can also be considered as a phase transition process involving initial nucleation at the interface between the electrode and electrolyte and subsequent growth from the interface towards the bulk of electrode. Lithium ion intercalation occurs *via* redox or Faradaic reaction which entails the reduction of valence state of the transition metal ions in the electrode. The "formula" intercalation maximum can be calculated according to the highest valence reduction. Taking MnO_2 for example, if the Mn^{4+} ions could be completely reduced to Mn^{2+}, the specific capacity of MnO_2 would be more than 600 mA h g^{-1}. However, this high capacity has never been observed in experiments, due to other limitations that need to be considered. The very first consideration would be reversibility. The extraction of lithium ions may become very difficult or practically impossible if a maximal amount of lithium ions are inserted, due to large positive enthalpy associated with the phase transition. So practically achieved maximal insertion capacity is dependent on the reversible phase transition boundary and is always much lower than the theoretical limit calculated from maximal valence reduction.[45] In addition, the insertion of lithium ions into the electrode host would induce a large volume change due to the change of crystal lattice and/or structure, resulting in a loss of mechanical integrity of the electrode.[46,47]

In order to accommodate more lithium ions than the theoretical limit, the reversible phase transition boundary of the bulk materials needs to be extended. The Faradaic reaction and the phase transition associated with lithium ion intercalation and de-intercalation is dependent on the nature of the electrode materials including the arrangement of ions, the type and level of

impurities and defects, and the surface energy. Electrodes away from equilibrium state may favor accommodating more lithium ions through reversible intercalation and de-intercalation process than the same materials in a thermodynamic equilibrium state. A number of ways could be used to create materials away from equilibrium. For example, nanostructured electrodes with huge surface energy are in a state far from thermodynamic equilibrium.[48] As a result, the reversible phase transition limit of lithium ion intercalation and de-intercalation is often extended with much greater lithium ion storage capacity. In addition to the improvement of energy storage capacity, nanostructures also improve kinetics by providing a short diffusion path for lithium ions and enhance the rate capability.[49,50] Nanostructures also permit freedom for volume change during long term cycles, alleviating the negative effect which could cause capacity degradation.[51,52]

Besides nanostructure, surface defects would contribute to lithium ion intercalation by shifting thermodynamics and improving kinetics. The presence of surface defects increases the surface energy and could possibly serve as nucleation center and, thus, facilitate phase transition. In addition, the presence of surface defects reduces the charge transfer resistance and improves the charge transfer kinetics while at the same time preventing active electrode dissolution in the electrolyte, which could improve cyclic stability.[53] After the surface charge transfer process, lithium ion diffusion from the surface into interior depends on the crystal structure as well, so crystallinity is another factor to consider and manipulate to enhance lithium ion insertion capability.[54] For some intercalation compounds, an amorphous structure appears to be more open to lithium ion diffusion due to the ability to withstand insertion stress with less well packed ions. Nanostructures, highly defective surfaces, and amorphous electrodes are all away from thermodynamically equilibrium states. Hence appropriately designed nano- and microstructures and the careful manipulation of surface and bulk chemistry will change the phase transition boundary, improve the transport kinetics, and permit more freedom for long-term cyclic stability.

In addition to searching and developing electroactive materials with higher lithium ion insertion capacity, rapid charge and discharge rate, and improved cyclic stability, research has been aimed at the development and fabrication of binderless electrode films (with directly incorporated conductive components) through solution-based chemical processing.[55,56] In such an approach, the commonly used polymer binders to improve the mechanical integrity of the electrodes could be eliminated and, thus, enhance the energy storage capacity of a battery, as well as simplify the fabrication process and possibly reduce the fabrication cost. In addition, the possible electrolyte permeation path blocking problem induced by excess binder, which would severely reduce the active power electroactivity, could be avoided.[57] Besides excluding binder from the electrode composition, some research groups also fabricated binderless and carbon-free thin film electrodes which promise a higher energy density because of the pure electroactivity of the electrode.[58–60] These thin film electrodes, circumventing routine but tedious electrode casting fabrication, have a bright application future as microbattery electrodes, and could be used in vast number of research areas since they could power micro-electronic devices.[61,62]

2. Nanostructured lithium ion intercalation electrodes

2.1 Nanostructured $LiFePO_4$ cathode and $Li_4Ti_5O_{12}$ anode

Generally speaking, nanostructures refer to structures with one or more dimensions confined in the scale between molecular and microscopic scope, *i.e.* 0.1–100 nm. Nanostructure has been a hot topic and intensively studied for the past decade because of its scientific significance. Nanostructured materials offer the unusual mechanical, electrical and optical properties endowed by confining the dimensions of such materials and the overall behavior of nanostructured materials exhibit combinations of bulk and surface properties.[63] Such materials have been applied in many engineering applications such as field-effect transistors,[64] chemical and biological sensors[65,66] and dye sensitized solar cells[67,68] to improve device performance (*e.g.* efficiency, capacity *etc.*). Lithium ion batteries is one of these fields that has benefited from the introduction of nanostructures: the application of nanostructured electrodes has significantly improved the lithium ion intercalation capability, *e.g.* storage capacity, intercalation rate and cyclic stability.[69,70] Considering the liquid/solid interface reaction characteristic of lithium ion intercalation followed by diffusion into electrode bulk, it is reasonable to expect that large surface area and short lithium ion diffusion path can ensure complete Faradaic reaction at the interface and facilitate the diffusion into the bulk. Thus nanostructured electrodes which meet these requirements are highly favorable as intercalation hosts instead of bulk electrodes consisting of micrometre sized particles.

$LiFePO_4$. $LiFePO_4$ is perhaps the best cathode example to illustrate the contribution of nanosized structures to facilitating lithium ion intercalation/de-intercalation. $LiFePO_4$ has been regarded as a good cathode material due to its appreciable capacity and moderate operating flat voltage, but suffered low electronic conductivity, which severely limited its practical application at higher powers.[71] To solve this problem, besides using carbon coating[72] or lattice doping[73] to improve the particle electronic conductivity, there have been numerous efforts of fabricating nanostructures to reduce the grain size of the samples and consequently the diminution of the diffusion length both for electrons and ions.[74] It has been readily recognized that rate capability of $LiFePO_4$ was mainly controlled by its specific surface area and nanostructured electrodes could well improve the rate capability.[75,76] In addition, nanostructured $LiFePO_4$ would have much larger contact area with the conductive carbon added when assembled into battery cells and thus possess better conductivity than bulk $LiFePO_4$.

The conventional route for fabricating $LiFePO_4$ powders was mainly through solid-state synthesis. The starting precursors consisted of stoichiometric amount of iron salt, a lithium compound and most commonly ammonium phosphate as phosphorus source. After heat treatment first at 300–400 °C to expel gases and followed by calcination at higher temperature up to 800 °C under inert or slightly reductive atmosphere, the $LiFePO_4$ powders could be obtained.[77] However, the obvious disadvantage of the conventional solid state method was the particle growth and agglomeration due to the high temperature

employed and the resultant product always possessed very small specific surface area.[78] To solve this problem, mechanochemical activation was introduced into the process and the resultant powders had a much larger specific surface area.[79] There have also been efforts using microwave heating instead of the furnace heating which limited the calcination temperature to a lower value to avoid excessive particle growth.[80] However, even with these modified methods, it was difficult to obtain $LiFePO_4$ with particle sizes below hundreds of nanometres.

Solution based methods have been proved to be effective for producing nanostructured $LiFePO_4$.[81] Hydrothermal method and sol–gel method were the two main methods employed and the obtained nanostructured $LiFePO_4$ exhibited noticeable intercalation capability improvement as compared with micrometre-sized $LiFePO_4$.

Hydrothermal growth refers to crystallizing substances at elevated temperature (typically 100–200 °C) from aqueous solutions at high vapor pressures. The starting precursors for fabricating $LiFePO_4$ were typically an iron salt such as $FeSO_4$, phosphate acid H_3PO_4 and lithium base LiOH.[82] Particles of sizes from tens of nanometres to hundreds of nanometres could be obtained by tuning the reaction time, temperature and pH value.[83] Dumbbell-like $LiFePO_4$ microstructures hierarchically constructed with two-dimensional nanoplates of ~300 nm length and ~50 nm thicknesses were fabricated *via* hydrothermal self-assembly and exhibited a stable discharge capacity of *ca.* 110 mA h g^{-1} over 70 cycles at a C/30 charge/discharge rate (Fig. 3).[84] Recham *et al.* used a solvothermal–hydrothermal method to enable the growth of $LiFePO_4$ with controlled size and morphology and the best sample with particle size of 300 and 500 nm could deliver a sustainable capacity of 150 mA h g^{-1} at a C/10 rate.[85] $LiFePO_4$ nanowires with diameters of a few hundred nanometres were fabricated by adding nitrilotriacetic acid and isopropanol to the precursors and could reach an initial discharge capacity of 150 mA h g^{-1} and retained still as high as 138 mA h g^{-1} after 60 cycles at a charge/discharge rate of 0.1 C.[86]

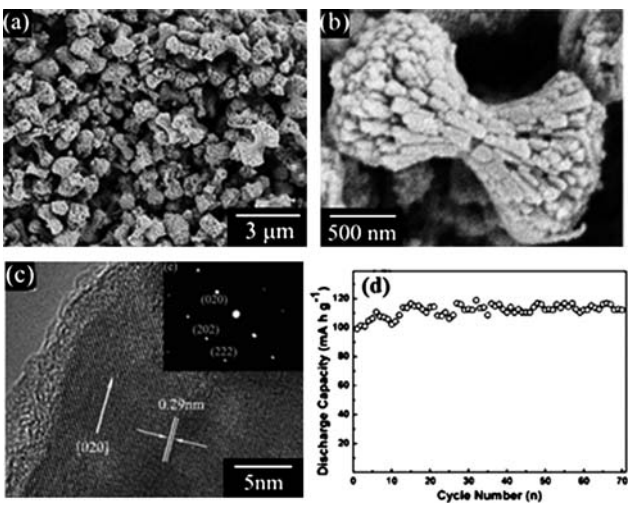

Fig. 3 (a) Typical low-magnification SEM image of dumbbell-like $LiFePO_4$, (b) an individual dumbbell-like $LiFePO_4$ from the obverse side, (c) HRTEM image of the tip of an individual dumbbell shape and (d) discharge capacity *vs.* cycle number of dumbbell-like $LiFePO_4$ at C/30 charge/discharge rate.[84]

The sol–gel route is another commonly used solution based method to fabricate nanostructured $LiFePO_4$. Porous nanostructured $LiFePO_4$ powder with a particle size distribution of 100–300 nm was obtained by using an ethanol based sol–gel route with lauric acid as a surfactant. The nanoparticles could deliver a specific capacity of 157 mA h g^{-1} at a discharge rate of 1 C and still had 123 mA h g^{-1} delivered when the rate was increased to 10 C.[87] Similar high rate capability for lithium ion intercalation was also reported on sol–gel prepared wired mesoporous $LiFePO_4$.[88]

For the hydrothermal and sol–gel methods, there has also been quite a lot of reported work on nanostructured $LiFePO_4$/C composites with carbon coating aiming at enhancement of electronic conductivity which had even better rate capability than single phase nanostructured $LiFePO_4$.[89–93] In addition to the hydrothermal and sol–gel method, co-precipitation,[94,95] emulsion-drying[96] and spray pyrolysis methods[97] could also be employed to fabricate nanostructured $LiFePO_4$ or $LiFePO_4$/C composites.

$Li_4Ti_5O_{12}$. The advantages of nanostructures were also demonstrated well in the study of $Li_4Ti_5O_{12}$ which is promising lithium ion battery anode material. $Li_4Ti_5O_{12}$ has a good cyclic stability due to zero strain or volume change during charging and discharging.[98] However, similarly to $LiFePO_4$, it also suffered from poor rate capability due to low electronic conductivity.[99] There has been much reported work focusing on fabricating different nanostructures to improve the performance of $Li_4Ti_5O_{12}$ at high powers. The lithium ion intercalation performance of $Li_4Ti_5O_{12}$ nanoparticles of two different sizes, *i.e.* 700 and 350 nm was studied. It was found that at room temperature, when the charge/discharge rate was increased above 1 C up to 5 C, the 350 nm sample exhibited a significantly higher capacity than the 700 nm sample and this difference increased as rate increased.[100] Jaiswal *et al.* fabricated $Li_4Ti_5O_{12}$ by pyrolysis of an aerosol precursor and the resultant nanoparticles had the size distribution between 50 and 200 nm and showed a high charge capability with values of 148 and 138 mA h g^{-1} at C/25 and 5C respectively.[101] Three-dimensional architectures of $Li_4Ti_5O_{12}$ nanofibers were fabricated *via* electrospinning and exhibited an initial capacity of 192 and 170 mA h g^{-1} at 0.5 and 1.5 C, respectively.[102] $Li_4Ti_5O_{12}$ nanowires were fabricated employing a solid-state reaction by calcining hydrothermally fabricated TiO_2 nanowires together with lithium acetate. The obtained $Li_4Ti_5O_{12}$ nanowires had an initial discharge capacity of 165 mA h g^{-1} at 0.1 C rate and retained 93% capacity even after a 10 C rate.[103] $Li_4Ti_5O_{12}$ hollow microspheres assembled by nanosheets were synthesized *via* a hydrothermal route followed by calcinations. They exhibited a high capacity of 131 mA h g^{-1} even at a very high rate of 50 C. Similar as $LiFePO_4$, there has also been much effort in making carbon coated $Li_4Ti_5O_{12}$ nanostructures which further improved the rate capability by optimizing the electronic conductivity.[104–106]

For $LiFePO_4$ cathode and $Li_4Ti_5O_{12}$ anode as discussed above, both possess good capacities at low charge/discharge rate but capacities degraded severely as the rate was increased due to the poor electronic conductivity. The introduction of nanostructures improved the intercalation kinetics by providing larger electrode/electrolyte contact area and reduced path for electron

transportation and lithium ion diffusion, resulting in noticeably improved capacities at high rates.

2.2 Nanostructured oxide electrodes

2.2.1 Nanosize effects on intercalation capacity. Besides improving intercalation performance at high powers, nanostructure was also found to enhance capacities at low powers which even exceeded the theoretical intercalation limits. Recent advancement of nano-ionics has revealed theoretical justification for enhanced storage capacity endowed by the large surface area of nanostructure: when the particle sizes approach nanoscale, particle surfaces and grain interfaces start to play a determining role in the thermodynamics and kinetics, and a pseudo-capacitive storage mechanism will occur by accommodating lithium ions on the surface/interface, which was not found in micron-sized particles.[107,108] In other words, besides the classical absorptive mechanism of lithium ion storage (insertion reaction), there will be another adsorptive mechanism (interfacial reaction) contributing to lithium ion storage capacity when particle sizes were below certain critical values, *e.g.* several nanometres.[109] As a result, in contrast to the bulk materials which were limited by classical phase transformation boundaries during lithium ion intercalation, the phase transition boundary of the nanostructure was modified and could possibly accommodate more lithium ions during insertion.[110,111] Interpreted in terms of chemical formula, it could be assumed that a reduction in particle size led to a higher lithium ratio in the equilibrium composition of lithiated electrode.[112] Wagemaker *et al.* have studied the phase diagram of lithium insertion process into micron-sized and nano-sized TiO_2.[113,114] They found that while in micron-sized particles the intercalation maximum was 0.55 Li per TiO_2, when the particle size was reduced to below 40 nm, the saturation maximum was increased to 0.7 Li per TiO_2. This was attributed to the single Li-rich phase in nano-sized particles as compared with micron-sized particles where Li-rich and Li-poor phase coexisted. Another convincing advantage of nanostructure comes from the contribution to kinetics and related intercalation rates. Diffusion time of lithium ions inside lithium transition metal oxides or transition metal oxides is proportional to the square of diffusion path length and so the reduction of electrode particle sizes from micrometre to nanometre will greatly improve the intercalation kinetics and enhance intercalation.[115]

2.2.2 One-dimensional nanostructured oxide electrodes. According to the number of confined dimensions, nanostructures are classified into zero-, one- and two-dimensional structures. Zero-dimensional nanostructures are confined (nanometre-sized) in every dimension and are often regarded as nanoparticles.[116] One-dimensional nanostructures are mainly nanotubes, nanowires, nanorods, nanobelts *etc.* nanosized in two dimensions (radial dimensions)[117] while a two-dimensional nanostructure is a thin film with only one dimension (thickness) nano-sized.[118] As lithium ion battery electrodes, nanoparticles face possible problem of mechanical disintegration during repeated cycling which made it very difficult to maintain good electronic contact between particles.[119] This problem was much less severe for one-dimensional nanostructures since the axial dimension provided nearly no limitation to mass and electron charge transportation. Template-based electrodeposition and hydrothermal growth appeared to be two most effective methods to fabricate one-dimensional nanostructures.

Template-based deposition involves deposition of the material of interest, or a precursor for that material, into the pores of a microporous template membrane. After deposition, the template will be eliminated by either chemical etching or thermal annealing. By using polycarbonate filtration membrane (PC) as template, Martin and co-workers have fabricated polycrystalline V_2O_5 nanorod arrays. In lithium ion intercalation property study, the resultant nanorods delivered three times the capacity of a thin-film V_2O_5 electrode at a high rate of 200 C.[120] Wang *et al.* have successfully fabricated single-crystalline V_2O_5 nanorods, nanotubes and Ni–V_2O_5 nanocables by employing electrophoretic deposition.[121–123] As-fabricated $V_2O_5 \cdot H_2O$ nanotube arrays demonstrated an initial high capacity of 300 mA h g^{-1}, about twice that (140 mA h g^{-1}) of the plain film of the same chemical composition. Ni–$V_2O_5 \cdot nH_2O$ core/shell nanocable arrays were prepared by a two-step electrodeposition method with Ni nanorod arrays fabricated by electrochemical deposition first and vanadium pentoxide shell deposited onto the surface of nickel nanorods through sol electrophoretic deposition. Compared with V_2O_5 nanorod arrays and sol–gel-derived V_2O_5 films, the specific power of the nanocable arrays was enhanced by 1–2 orders of magnitude as shown in Fig. 4. Similar template-based sol–gel deposition employing PC template was also used for the synthesis of MnO_2 nanorods and the produced nanorods delivered an initial capacity of 183 mA h g^{-1} and stabilized on subsequent cycles to 134 mA h g^{-1}.[124]

The hydrothermal method is an effective method to fabricate one-dimensional nanostructures. Nanostructured α-, β- and γ-MnO_2 have been synthesized through the solution and hydrothermal route.[125] While α- and γ-MnO_2 nanowire or

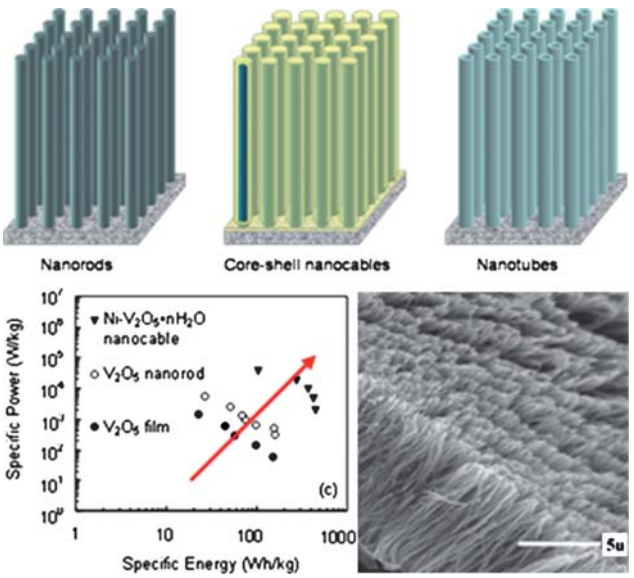

Fig. 4 Schemes of nanorod, nanotube and nanocable array electrodes for energy storage (top). SEM images of oxide nanorod arrays (bottom right) and comparison of specific energy and specific power of vanadium pentoxide electrodes in the form of film, nanorod arrays and nanocable arrays (bottom left).[123]

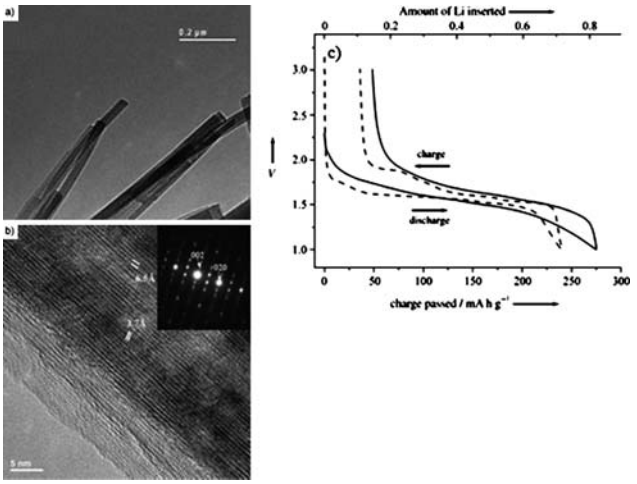

Fig. 5 (a) Low-resolution TEM image of the TiO_2-B nanowire, (b) high-resolution lattice image viewed down the [100] projection (inset: electron diffraction pattern of a TiO_2-B nanowire and (c) variation of potential (*vs.* 1 M Li^+/Li electrode) with Li content (charge passed) for TiO_2-B nanowires (solid line) and bulk TiO_2-B (dashed line) cycled under identical conditions. Rate: 10 mA g^{-1} (10 mA of charge passed per gram of TiO_2-B); voltage limits: +1 and +3 V; V = potential.[127]

nanorods exhibited good electroactivity to lithium ions by delivering capacities more than 200 mA h g^{-1}, β-MnO_2 nanostructures showed low capacity and poor cyclic stability. Other research indeed revealed that until reaching a small enough scale of particle size, the intercalation capacity of β-MnO_2 was fairly low.[126] TiO_2 is one of the most "hydrothermally fabricated" compounds used for lithium ion intercalation application. TiO_2 nanowires synthesized by hydrothermal method were reported by Armstrong *et al.* and the TEM images of the nanowires with the chronopotentiometric curves of lithium ion intercalation are shown in Fig. 5. The intercalation capacity was as high as 275 mA h g^{-1}, corresponding to the lithiation of $Li_{0.82}TiO_2$.[127,128] Nanorods and nanotubes of TiO_2 were also fabricated by different groups and exhibited similar high capacities comparable to TiO_2 nanowires.[129–131]

2.2.3 Template-based mesoporous oxide electrodes. Despite the reported high lithium ion intercalation capacities of one-dimensional nanostructures, the capacity stability in long term cycles was still a problem, *i.e.* capacity degradation was noticeable. There was always volume expansion/contraction of host structure accompanying lithium ion intercalation/de-intercalation which could damage the structure integrity and easily cause capacity fading.[132] There have been many efforts to design structures that could withstand volume change while maintaining cyclic stability. Mesoporous structures appear to be one of the most favorable choices. Mesoporous structure refers to nanostructures embedded with pores sized between 2 and 50 nm. They can sustain the volume change during lithium ion intercalation/de-intercalation due to the buffering role of mesopores to alleviate the strain.[133] In addition, since the electrolyte is stored in mesopores interspersed on the active solid matrix, mesoporous structure also preserved the short diffusion path for both lithium ions and electrons which permitted a better performance at large charge/discharge rates as compared to bulk materials.[134]

The fabrication of mesoporous nanostructures often involves the use of soft (surfactant) or hard templates. In the 1990s, surfactant-templated TiO_2 was initially fabricated by using amphiphilic poly(alkylene oxide) triblock copolymer as the structure-directing agent in an ethanolic solution of $TiCl_4$.[135] Later application of this mesoporous structured compound as lithium ion intercalation electrodes revealed unusually fast capacitive and intercalation charging abilities.[136] Besides the synthesis route just described, mesoporous TiO_2 could also be synthesized by the evaporation-induced self-assembly procedure with novel poly(ethylene-*co*-butylene)-*b*-poly(ethylene oxide) polymer (KLE) used as template. The templated films after annealing at elevated temperatures transform to the anatase phase and can store a capacity of *ca.* 200–250 mA h g^{-1}.[137] The rate capability measurement was also carried out on mesoporous TiO_2 fabricated by using amphiphilic molecule as the templating agent: the mesoporous samples delivered a capacity of 184 mA h g^{-1} at C/5 and 95 mA h g^{-1} at 30 C, possessing a much better rate capability than commercial samples.[138] Lou *et al.* studied the storage properties of TiO_2 mesoporous hollow particles and after the initial high capacity of 408 mA h g^{-1}, the capacity stabilized at >170 mA h g^{-1} for 35 cycles.[139]

Mesoporous V_2O_5 was fabricated following similar surfactant-templated procedures by using VCl_4 instead of $TiCl_4$. At a very high charge/discharge rate of 50 C, the capacity delivered by mesoporous V_2O_5 could be as high as 125 mA h g^{-1}, which promised its application as a low power capacitor or high power batteries owing to the good balance between specific power and specific energy.[140]

Besides using surfactant as soft template, mesoporous structure could also be obtained by using a hard template, *e.g.* mesoporous silica. Hollow $LiFePO_4$ was fabricated by using the hard templates KIT-6 and had a large BET specific surface area of 103 m^2 g^{-1} with pore size distribution centered at 5.6 nm.[141] The mesoporous electrode demonstrated excellent rate capability and cyclic stability. At a rate of 15 C, the capacity was 153 mA h g^{-1}, 95% of that at 0.2 C rate. In addition, no obvious capacity degradation was noticed after 80 cycles. Considering the well-known low rate capability of $LiFePO_4$ due to its poor electronic conductivity, using mesoporous structured electrodes could be one of the possible solutions to solve this problem.

Besides the improved electrode cyclic stability and enhanced rate capability, for some compounds, the electroactivity was significantly enhanced after changing the bulk material into a mesoporous structured one. Successful fabrication of mesoporous β-MnO_2 employing mesoporous silica KIT-6 was reported. While bulk β-MnO_2 was for a long time assumed to be with extremely low intercalation capacity, *i.e.* below 60 mA h g^{-1},[126] mesoporous β-MnO_2 with a pore size centered at 3.65 nm exhibited a high capacity of 284 mA h g^{-1} and stabilized at 200 mA h g^{-1} after initial degradation at a current density of 15 mA g^{-1}.[142] The TEM and HRTEM images of the mesoporous β-MnO_2 before and after cyclic reactions together with the electrochemical cyclic performance are shown in Fig. 6 and it could be clearly seen that the integrity of mesoporous structure was well maintained during the intercalation/de-intercalation cycles. This mesoporous electrode also possessed good rate

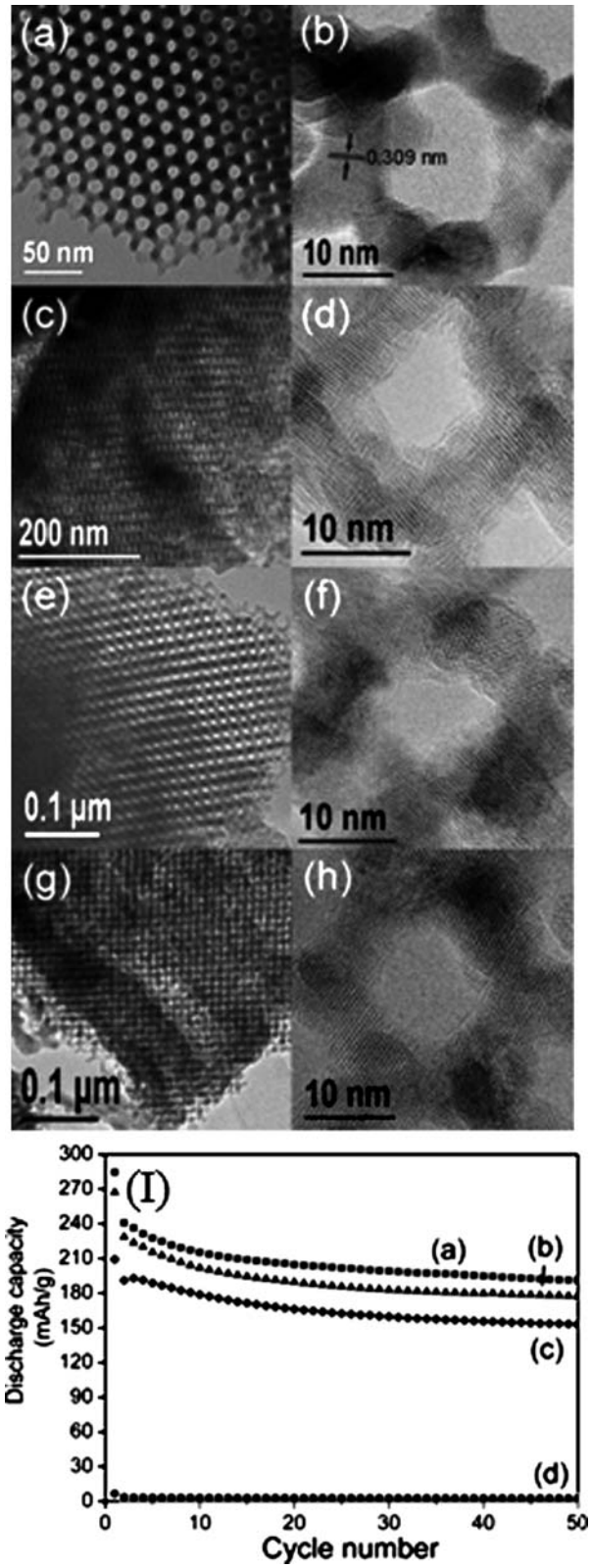

Fig. 6 TEM and high-resolution TEM (HRTEM) images of mesoporous β-MnO_2: (a, b) as-prepared; (c, d) after first discharge; (e, f) end of discharge after 30 cycles; (g, h) end of charge after 30 cycles and (i) cyclic retention for mesoporous β-MnO_2 cycled at (a) 15, (b) 30 and (c) 300 mAg^{-1}; (d) bulk β-MnO_2 cycled at 15 mA g^{-1}.[142]

capability by having 81% capacity remaining after the current density was increased to 300 mA h g^{-1}. Mesoporous $LiMn_2O_4$ was made through a similar route by employing KIT-6 template but involved more solid-state reactions to evolve from Mn_2O_3 to $LiMn_2O_4$.[143] Thus-obtained mesoporous $LiMn_2O_4$ nearly doubled the capacity of bulk $LiMn_2O_4$ and possessed a much better cyclic stability than nanoparticulate $LiMn_2O_4$. The surface area of these two mesoporous products were 127 and 90 m^2g^{-1}, respectively.

In conclusion, during lithium ion intercalation/de-intercalation, mesopores readily supplied ions from the electrolyte and acted as the buffering layers to alleviate the volume change experienced during lithium ion intercalation/de-intercalation. As a result, the cyclic stability of mesoporous structured electrodes was improved and the rate capability was enhanced. Using a template-based method to fabricate mesoporous structure could produce ordered pores with sizes controllable by template tuning. In general, the BET specific surface areas of template-derived mesoporous structures are >90 m^2 g^{-1} and the pore sizes were centered from 3–6 nm. This structure is highly favorable for lithium ion intercalation as evidenced by noticeable improvement in capacities, cyclic stability and rate capabilities. However, the introduction of template into the synthesis processes induced much higher cost and the elimination of template after reactions was also a technical challenge. Recently, successful fabrication of high surface manganese dioxide following the template-free concept has been reported by Sinha *et al*. by means of a wet precipitation method[144] and its application in extensive air purification turned out to be a great success. However, because of the unordered mesoporosity, manganese dioxide fabricated in this way was not suitable as a large lithium-ion capacity storage device since the electrolyte penetration would be very difficult in such thick oxide films with small pores. For unordered mesoporosity, the availability of macropores is crucial to facilitate complete electrolyte infiltration into the random distributed mesopores. Various attempts have been reported in fabricating a variety of macroporous metal oxides, *e.g.* NiO nanoflowers.[145] The combination of macroporous and mesoporous structure was also reported in V_2O_5[146] to improve lithium-ion intercalation kinetics. In our experiments, we have successfully deposited hierarchically mesoporous MnO_2 nanowall arrays onto a platinum substrate to make thin film electrodes and obtained excellent capacities and cyclic stability which will be discussed in detailed in section 5.3.

2.3 Problems of nanostructured electrodes

However, nanoscale is altogether positive and there are also some drawbacks associated with nanostructured electrodes which are extremely severe for certain electrodes. One problem was related with solid electrolyte interface (SEI) growth on the electrode surface. SEI was formed mainly by lithium containing organics and inorganics decomposed from the electrolyte solvents and salts before or in the initial cycles and could help stabilize the electrode/electrolyte interface by reducing the direct contact between the electrode and electrolyte and preventing further electrolyte decomposition.[147,148] SEI was discerned on graphite anode as the electrode/electrolyte stabilizer and contributed to the capacity retention in long cycles despite that

there was a large irreversible capacity caused by its formation.[149,150] However, the SEI layer had very low ionic conductivity and electronic conductivity; the formation process was also accompanied by heat generation which would cause thermal shifting from the stable conditions.[151] Excessive formation of an SEI layer on the electrode surface could cause thermal instability, *e.g.* temperature elevation and hinder intercalation kinetics, causing noticeable irreversible capacity (low coulombic efficiency).[152] In addition, the excessive formation of an SEI layer could also consume considerable amount of lithium ions in the electrolyte, causing obvious capacity degradation.[153,154] The most important factors determining the formation of SEI were the electrolyte used and electrode morphology.[155,156] Owing to the large surface area and corresponding large electrode/electrolyte interface, SEI formation on nanostructured electrodes was often far more noticeable than on bulk electrodes and often accompanied by formation of thicker and more compact layers with much more heat produced.[157] Taking $LiCoO_2$ cathode for example, it was found that $LiCoO_2$ with smaller particle size was identified with a thicker SEI layer which acted as a barrier for Li-ion diffusion and resulted in deteriorated rate capabilities at higher C rates.[158] A similar problem was also identified on a $LiMn_2O_4$ cathode and the increase of SEI layer thickness directly caused capacity fading in long term cycles.[159,160]

Another problem of nanostructured electrodes was related with the active metal ion dissolution in the electrolyte which would cause capacity degradation. $LiMn_2O_4$ was one typical victim: Mn ions in the electrode could easily dissolve in the electrolyte and the large electrode/electrolyte interface characteristic of nanostructures badly aggravated this problem.[161,162] Despite that the discharge capacity and rate capability could possibly be improved, cyclic stability was obviously a big problem for nanostructured lithium manganese oxide and related manganese oxide electrodes.[125,163]

To solve the excessive SEI growth and active metal ion dissolution problems, special surface chemistry design is necessary for nanostructured electrodes as we are going to discuss next.

3. Surface chemistry engineering

3.1 Surface coating on electrodes

As just discussed, nanostructures have been proved highly effective in enhancing the electrode intercalation capability. The importance of the electrode and electrolyte interface was also recognized especially when the electrode dimension approached the nanoscale. However, for all the intercalation electrodes including nanostructured electrodes, there are two problems that need to be solved: (1) the first step of lithium ion intercalation into the electrode involved the charge transfer process of lithium ions from the electrolyte onto the surface of electrode and entailed redox reactions involving the participation of electrons. If the extra charge could not be readily transferred away after reaction, charge accumulation would occur to impede more reactions.[164,165] To ensure complete redox reactions, good charge transfer conductivity must be guaranteed; (2) during the long-time repeated intercalation/de-intercalation cycles, the electrode surface could possibly dissolve into the electrolyte and this problem was more severe for nanostructured electrodes because of the large solid/liquid interface.[166,167] The failure to maintain surface morphology integrity would directly lower intercalation capability, causing capacity degradation. Considering these two points, electrodes should possess good charge transfer conductivity and surface integrity over long-term cycles to ensure favorable intercalation capacity and cyclic stability.

Introducing other elements into the electrode compound was adopted as one way to enhance the surface charge transfer conductivity. The element would either substitute the transition metal ions (doping) to modify the crystal structure[168] or interact with the transition metal ions on the crystal surface without entering the lattice.[169] The charge transfer resistances in both situations were significantly reduced and the rate capability was obviously improved. However, despite the enhancement of surface charge transfer conductivity, the dissolution of electrode in the electrolyte was still a challenge to the performance stability of the nanostructured electrode.

To protect the electrode from dissolution, the straightforward but essential concept was based on reducing the direct contact between electrode and electrolyte, which could be realized by the method of coating a layer of porous materials on the electrode surface. The commercialized $LiCoO_2$ was used by many research groups as the model electrode to carry out the coating experiments and many oxides have been tested as the coating layer, *e.g.* Al_2O_3,[170] $AlPO_4$,[171] CeO_2,[172] TiO_2,[173] $Li_4Ti_5O_{12}$[174] *etc.* Fig. 7 shows a TEM image of coated $LiCoO_2$ and compares the

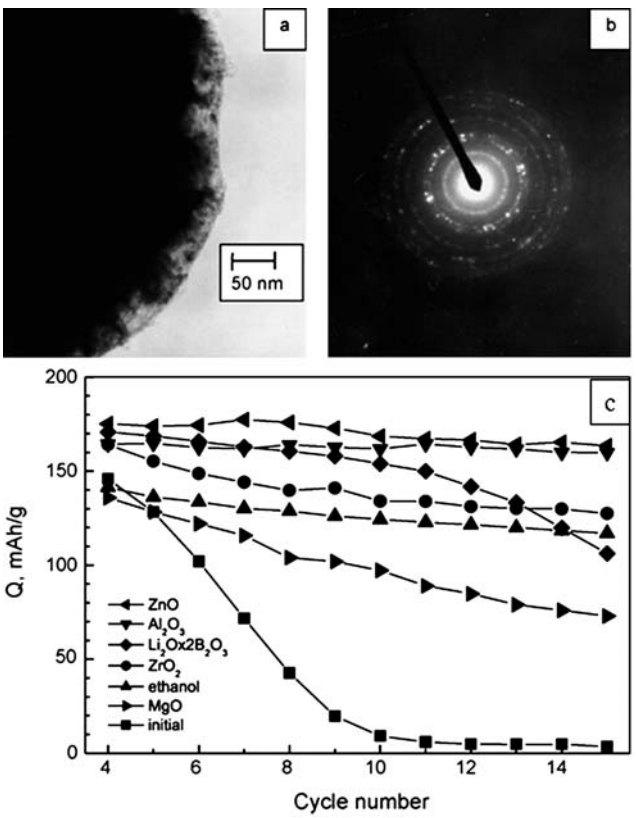

Fig. 7 (a) TEM image of $LiCoO_2$ surface modified with Al_2O_3, (b) electron diffraction of the coated $LiCoO_2$ and (c) discharge capacity of bare and surface modified $LiCoO_2$ *vs.* cycle number.[175]

electrochemical cyclic performance comparison of the bare electrode and coated electrodes. It could also be seen that after coating, the cyclic stability of lithium ion intercalation measurements were obviously improved.[175] More detailed experiments were also carried out by using different techniques to coat TiO_2 onto the $LiCoO_2$ electrode surface and it was found that the mechano-thermal coating from pre-formed nanoparticles were preferable to sol–gel coating from an alkoxide precursor, the cyclic stabilities in both situations were noticeably improved (5-fold for sol–gel coating and 12-fold for mechano-thermal coating).[176] Besides acting as the protection layer to prevent electrode dissolution, the TiO_2 coating was also found to help suppress the cycle-limiting hexagonal/monoclinic/hexagonal phase transitions accompanying the charge–discharge processes. In addition to oxides coating, polymer coating was also experimented with a combined model calculation.[177] Electrochemical measurements showed that coating $LiCoO_2$ with a poly-(2EHA-Co–F) film significantly decreased the activation energy for Li^+ exchange which could improve reaction kinetics and facilitate the charge transfer process. Spinel $LiMn_2O_4$ or substituted $LiMn_2O_4$ is a promising cathode material but for a long time suffered rapid capacity fading during repeated charge/discharge cycles partly due to the dissolution of active Mn ions in the electrolyte especially when the electrodes were comprised of nanoparticles.[178,179] The Mn dissolution phenomenon was even more severe at elevated temperatures,[180,181] *e.g.* 55 °C. It turned out that coating oxides onto the electrode surface to reduce the direct contact between spinel and the electrolyte was an effective method to improve the cyclic stability of $LiMn_2O_4$. Kannan and Manthiram coated $LiMn_2O_4$ with Li_xCoO_2, $LiNi_{0.5}Co_{0.5}O_2$, Al_2O_3 and MgO using solution-based coating followed by heat-treatment.[182] All the surface coated (modified) samples showed much better capacity retention at both room temperature (25 °C) and elevated temperature (60 °C) than unmodified $LiMn_2O_4$. The $LiNi_{0.5}Co_{0.5}O_2$-modified sample showed superior capacity retention with only 2.8% fade in 100 cycles at 60 °C with capacity around 110 mA h g^{-1}; the Al_2O_3 modified sample showed a higher capacity of 130 mA h g^{-1} but with a faster fading rate (16% fade in 100 cycles at 60 °C); the $Li_{0.75}CoO_2$ modified sample showed the best combination of capacity (124 mA h g^{-1}) and retention (8% fade in 100 cycles at 60 °C). Because of easy synthesis and chemical stability, Al_2O_3 was the most used coating compound onto electrodes. There have also been several coating methods of Al_2O_3 such as melting impregnation,[183] reactive sputtering[184] and solution soaking:[185] noticeably improved cyclic stability of electrode being coated over uncoated one was observed. ZnO coating on $LiMn_2O_4$ was also reported and at elevated temperature of 55 °C, the coated $LiMn_2O_4$ showed capacity retention of 97%, significantly higher than the 55% capacity retention of the bare $LiMn_2O_4$.[186] The ZnO coating collected HF from the electrolyte and better preserved the interfacial morphology and ensured the stable charge transfer process. A similar ZrO_2 coating also improved the high-temperature cyclic stability by screening the acidic species from the active electrode;[187] in addition, ZrO_2 coating improved the rate capability up to the high rate of 10 C owing to the enhanced charge transfer conductivity because coated ZrO_2 can act as a highly Li-conducting solid electrolyte interface and the strong bonding to $LiMn_2O_4$ which could tolerate the lattice stress resulting from the volume expansion during lithium ion intercalation.

Compared with the coatings onto $LiCoO_2$ and $LiMn_2O_4$ electrodes, the favorable coating compounds onto $LiFePO_4$ electrodes were limited to conductive species. Because of the poor electronic conductivity of $LiFePO_4$, the bare electrode could only be charged/discharged at a very low rate.[188,189] Thus the adopted coating must be highly conductive in order not to aggravate the low rate performance problem of the electrode. The conductive coatings on $LiFePO_4$ were mainly three kinds of conductive compounds: carbon coating,[190,191] metal coating[192,193] and conductive oxide coating.[194] Fig. 8 shows the TEM images and electrochemical cyclic performance at different charge/discharge rates of $LiFePO_4$/C nanoplate coated by amorphous carbon.[195] It could be seen that the coated electrodes exhibited excellent cyclic stability and the discharge capacity was still about 100 mA h g^{-1} at a high rate of 10 C, preserving more than 50% of the discharge capacity at 0.1 C.

For transition-metal oxide electrodes, carbon or metal was often used as coating layers, VO_x coated with carbon prepared *via* reaction under autogenic pressure at elevated temperatures was reported.[196] Both the reversibility and rate capability was much better than V_2O_5 nanoparticles without carbon coating. Metal layers were also coated onto nanostructured TiO_2: the silver mirror reaction was used to coat Ag particles onto hydrothermally synthesized TiO_2 nanotubes and cyclic stability and rate capability was found to be improved.[197] A metal film of

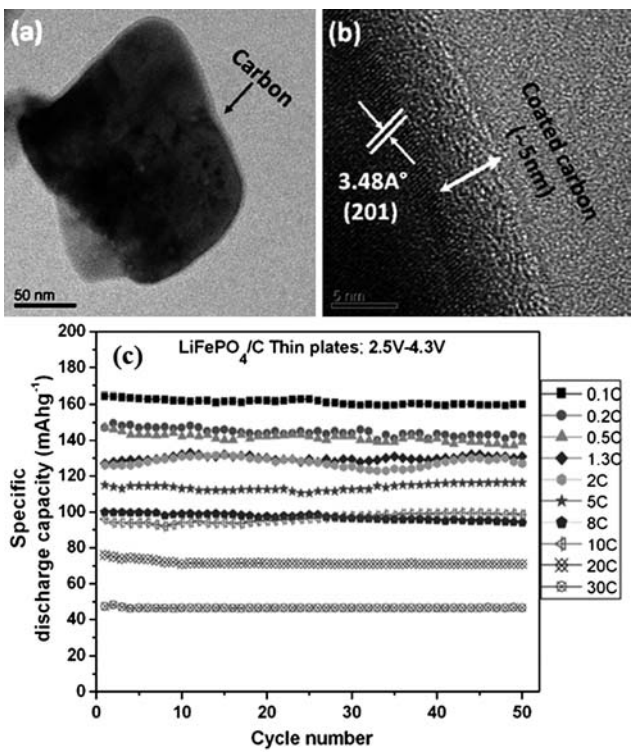

Fig. 8 (a) TEM image showing a uniform coverage of amorphous carbon coating around the surface of a $LiFePO_4$/C nanoplate, (b) HRTEM image showing a nearly 5 nm thick amorphous carbon layer around the surface of $LiFePO_4$/C and (c) capacity *vs.* cycle number plots of $LiFePO_4$/C thin nanoplates at various current rates of 0.1 to 30 C.[195]

Cu or Sn was vacuum-deposited onto the surface of mesoporous anatase TiO_2 electrodes and the electrode surface modification made by thin-film deposition improved the kinetics of Li intercalation/de-intercalation and remarkably enhanced the electrochemical performances in terms of capacity, stability and rate capability.[198]

Derived from the coating concept, recently a new method of surface grafting was developed to modify the surface chemistry, or say, to lower the interfacial chemical reactivity of side reactions (*e.g.* electrolyte decomposition) which was detrimental to long-term energy storage properties. Nitro-aryl groups were electrografted onto a $Li_{1.1}V_3O_8$ surface by *in situ* diazonium chemistry during lithium ion intercalation when the electrode was potentiodynamically discharged.[199] A homogeneous multilayer was formed whose thickness could be modulated. The multilayer did not impede charge transfer or limit the electrochemical reactivity. However, it did decrease the chemical reactivity of the material towards the electrolyte, resulting in significant improvements of the capacity retention.

To date, coating appears to be the most effective method to improve the surface charge transfer process. However, whatever kind of coating techniques was used, the coating process is often complicated and sometimes involved delicate equipment to achieve a homogeneous coating layer with good porosity. The basic requirement of the electrolyte permeability after coating was always challenging and tricky to meet. Considering all of these practical problems, we have been attempting to create a layer of surface defects on the intercalation electrodes to play a similar role as an exterior coating. The work included TiO_2 nanotube arrays and V_2O_5 xerogel films annealed under reducing or inert gas flow and identified with surface defects (section 3.2 and 3.3).

3.2 Enhanced rate capability of TiO_2 nanotube arrays with surface defects

The lithium ion intercalation and de-intercalation is a heterogeneous reaction which takes place at the interface between the solid electrode and liquid electrolyte; the surface chemistry and defects are, therefore, expected to play an important role in catalyzing or retarding the interface reaction and promote or prevent the nucleation. Appropriate surface chemistry and defects are expected to lead to enhanced lithium ion storage capacity and possibly improved kinetics.[200] Surface chemistry and defects can be modified through various means such as surface coating, self-assembly of a monolayer, and injection of impurity species. Reacting the surface with reactive gas at elevated temperature would be a simple and easy way to accomplish such surface modification. TiO_2 nanotube arrays annealed in CO gas serves as an example to illustrate the influence of surface defects on the lithium ion intercalation properties as described below.

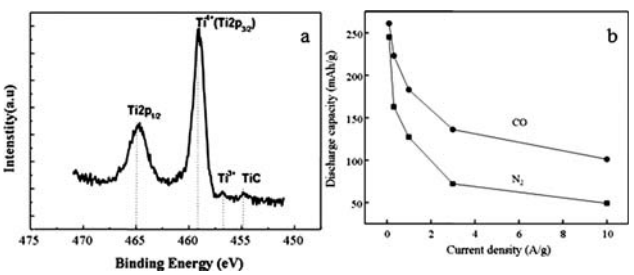

Fig. 9 (a) Ti 2p XPS spectra of TiO_2 nanotube arrays annealed in CO gas at 500 °C with carbon doped Ti–C species and Ti^{3+} state available and (b) the initial discharge capacities of TiO_2 nanotube arrays annealed in N_2 and CO at 400 °C for 3 h as a function of applied discharge current densities. The measurements were carried out in a potential window between −0.6 and −2.1 V *vs.* Ag/AgCl as a reference electrode.[202]

Titania nanotube arrays were synthesized by anodic oxidation method according to literature.[201] Then they were annealed in reducing CO gas at 400 °C for 3 h.[202] XPS study of the nanotube arrays annealed in CO gas confirmed carbon doping onto TiO_2 surface in the form of a minor amount of Ti–C and the formation of Ti^{3+} point defects as shown in Fig. 9a. Compared with N_2-annealed arrays which possessed an electrode resistance of 66 Ω and a charge-transfer resistance of 38 Ω, CO annealed arrays possessed an electrode resistance of 60 Ω and a reduced charge-transfer resistance around 26 Ω, indicating a higher charge-transfer rate of Li^+ in the electrode. This improved charge-transfer conductivity of CO annealed TiO_2 arrays could be attributed to the presence of surface Ti–C species and Ti^{3+} groups with oxygen vacancies which enhanced the surface conductivity of the electrode.

Fig. 9b summarizes and compares the relationship between the discharge current density and corresponding intercalation capacity of the TiO_2 nanotube arrays annealed in N_2 and CO, respectively. The lithium ion intercalation capacity of the N_2 annealed nanotube arrays was found to be more sensitively dependent on the current density; the intercalation capacity reduced rapidly with the increased current density. At a current density of 100 mA g^{-1}, the capacity of the N_2 annealed TiO_2 nanotube array was as high as 245 mA h g^{-1}. However, when the current density was tripled to 320 mAg^{-1}, the capacity decreased to 164 mA h g^{-1}, losing one third of its discharge capacity. At a current density of 1 Ag^{-1}, the capacity was further reduced to a value of 127 mA h g^{-1}. In comparison, the CO annealed TiO_2 nanotube arrays demonstrated less sensitive intercalation capacity. For example, an intercalation capacity of 261 mA h g^{-1} decreased to 223 mA h g^{-1}, less than 20% reduction, when the current density increased from 100 to 320 mA g^{-1}. It was clear that the CO annealed TiO_2 nanotube arrays possessed much higher intercalation capacities, approximately double of that of N_2 annealed TiO_2 nanotube arrays at high current densities, *i.e.* possessing a capacity of 101 mA h g^{-1} at 10 A g^{-1}.

The presence of defects may contribute to the improved intercalation capability of the CO annealed TiO_2 nanotube arrays, as has been reported in other intercalation oxide electrodes such as V_2O_5.[203] In the titania system, both intercalation and de-intercalation processes involve a phase transition between tetragonal TiO_2 and orthorhombic Li_xTiO_2 through the following reaction:

$$xLi^+ + xe^- + TiO_2 = Li_xTiO_2$$

Phase transition occurs through nucleation at the interface and subsequent growth from the interface towards the interior. Besides improving the charge transfer conductivity, the presence

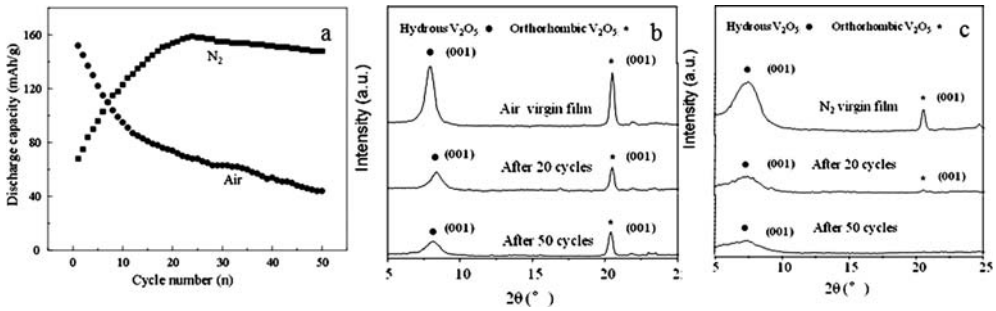

Fig. 10 (a) The Li-ion intercalation discharge capacity of V_2O_5 films annealed in air and N_2 at 300 °C for 3 h as a function of cyclic number. The measurements were carried out in a potential window between 0.6 and −1.4 V *vs.* Ag/AgCl as the reference electrode at a current density of 600 mA g^{-1}; X-ray diffraction patterns of V_2O_5 films annealed in (b) air and (c) nitrogen before and after 20 and 50 cycles of lithium ion intercalation and de-intercalation measurements.[204]

of defects on the surface of TiO_2 nanotubes could also serve as nucleation sites so as to promote the phase transition and enable more lithium ion intercalation and improve the rate capability.

3.3 Improved cyclic stability of V_2O_5 xerogel film with surface defects

Appropriately introduced surface defects could not only enhance the rate capability of electrodes but also improve the cyclic stability. The study of V_2O_5 xerogel films treated in nitrogen gas revealed the contribution of surface defects to improved cyclic stability.

Sol–gel derived V_2O_5 films on FTO glass were annealed in N_2 and air-flow atmosphere at 300 °C for 3 h under otherwise identical conditions.[204] While air annealing did not change film color much; after N_2 annealing, the originally yellow film turned dark green suggesting the presence of V^{4+} and V^{3+} species on the film surface. The charge transfer resistance of the N_2-annealed film was two thirds that of the air-annealed film, reduced from 125 to 86 Ω. Fig. 10 compares the long term cyclic stability and corresponding XRD patterns of the air- and nitrogen-annealed films for lithium ion intercalation measured with a current density of 600 mA g^{-1} for 50 continuous discharge/charge cycles. The poor cyclic stability of air-annealed V_2O_5 film could be caused by the relatively larger grain size.[205] For N_2-annealed film, before reaching the highest discharge capacity value of 158 mA h g^{-1} at the 24th cycle, it started with a low discharge capacity of 68 mA h g^{-1}. After 50 cycles, the capacity was still as high as 148 mA h g^{-1}. While the mechanism causing such a change in storage capacity, with initially low followed by a sharp increase with increased lithium ion intercalation and de-intercalation cycles in the N_2-annealed sol–gel derived V_2O_5 film electrodes, is not clear, the same or similar results or observation have been reported in literature and it could possibly be due to the surface defects.[206,207] The crystallinity of these two kinds of films were also found to change differently during cycling: while the hydrous V_2O_5 peak degraded noticeably in the air-annealed film, such degradation was much less severe in the N_2-annealed film, suggesting the disruption of layered structure. Along with defects on the film surface, the integrity of layered structure could be a further reason for the good cyclic stability of the N_2-annealed film.

The presence of surface defects could contribute significantly to the stability improvement which can be analyzed in three aspects: (1) the interfacial charge transfer abilities of the N_2-annealed V_2O_5 film was improved because of the presence of more conductive surface defect species. As has been found in the optical absorption and impedance analysis, both the optical and electrical conductivity of the film annealed in N_2 was improved compared with film annealed in air due to the presence of V^{4+}, V^{3+} ions and associated oxygen vacancies on the film surface. It was found that the intercalation capability of lithium ions into the V_2O_5 xerogel film annealed at high temperature was mainly determined by the interfacial reactions at the electrolyte/electrode interface rather than the lithium-ion transport in the bulk oxide electrode.[208] Since the enhanced charge transfer conductivity facilitated electron transportation during lithium ion intercalation/de-intercalation at the electrolyte/electrode interface which would obviously facilitate the lithium ion intercalation process,[209] the cyclic stability and rate capability improvement could be explained. Similar improvement after N_2 annealing was also observed in TiO_2 nanotube arrays;[210] (2) in addition to the conductivity enhancement contribution, the defect layer, like coating layers, also prevented the possible dissolution of V_2O_5 film in the electrolyte and ensured the integrity of film surface morphology upon cycling. One of the major causes of lithium ion intercalation capacity degradation in long-term cycles was the dissolution of the active material (electrode) in electrolyte. Building up a protecting layer on the surface will effectively reduce the possibility of electrode dissolution, thus improving the cyclic stability; (3) more than just a simple protecting layer, these surface defects of lower vanadium valency and oxygen vacancies could also serve as nucleation centers in the phase transformation process that occurred during lithium ions intercalation/de-intercalation.[211] For this reason, the phase transformation process in the N_2-annealed film was much easier and more reversible. The crystal structure was also more stable and the stability of lithium ion intercalation capacities was better than for air-annealed V_2O_5.

4. The crystallinity effect on lithium ion intercalation

4.1 Amorphous structure with high energy storage capacity

After initial interfacial charge transfer reactions, lithium ions will diffuse into the bulk through the open spaces inside the crystal structure of electrodes. With similar diffusion length, the

diffusion kinetics is dependent on crystal structure order—the crystallinity—that could be estimated by examining X-ray diffraction patterns. Well-crystallized structures have long-range atom order while amorphous structures lack even short range order. Intuitively, long range ordered structure is good for lithium ion diffusion because of the absence of possible collisions with host atoms which impedes lithium ion transport; however, the rigid crystalline structure is also fragile to lattice expansion and means that the insertion of lithium ion, which definitely would induce strain, would cause irreversible deformation to the crystal structure and very detrimental to the reversibility of lithium ion intercalation/de-intercalation.[212] In contrast, an amorphous structure with characteristic loose packing of atoms might possibly permit more diffusion freedom due to the ability to withstand more structure deformation.[213]

The higher capacity of amorphous/low crystallinity substances over crystalline ones was reported and discussed as early as the study of intercalation cathode sulfides, *e.g.* MoS_2. Whittingham *et al.* pointed out that this might be associated with either the more open lattice in amorphous compounds or the disordered framework which prevented the decomposition in some materials.[214] In terms of nano-ionics, amorphous compounds have more interfaces within the crystal due to the small grain size and could store more lithium ions than well-crystallized compounds on the grain boundaries and interfaces. The low mobility of lithium ions inside the amorphous structure could be a limitation for high rate performance but the high energy storage capacity was indeed promising for powering small electronics. Especially given that the energy storage capacity of cathodes has not seen much impressive improvement in recent years, constructing appropriate amorphous structure might be a good direction to achieve high intercalation capacity and even high energy storage density.

Lithium transition metal oxides are often synthesized through high-temperature solid-state reactions, so the products were well crystallized structures like the layered structure of $LiCoO_2$, spinel structure of $LiMn_2O_4$ and olivine structure of $LiFePO_4$. However, for transition metal oxides which only consist of metal ions and oxygen, the variation of crystallinity was more controllable and the amorphous structure could be fabricated from low-temperature synthesis route.

Xu *et al.* synthesized amorphous manganese dioxide *via* a sol–gel route and the as fabricated material delivered a high capacity of 436 mA h g^{-1} and stored energy at a level of 1056 mW h g^{-1}.[215] However, the rate capability of this amorphous material was low due to the poor diffusion abilities of lithium ion inside the structure. To improve the rate capability, Xu *et al.* also made a cryogel from the sol–gel derived MnO_2 aerogel *via* freeze drying. The nanoporous cryogel had a high specific surface area of 350 m^2 g^{-1} and exhibited specific capacities of 289, 217 and 174 mA h g^{-1} at C/100, C/5 and 2 C rates, respectively, which demonstrated excellent rate capability.[216] West *et al.* fabricated amorphous MnO_2 nanowires arrays through a template-based electrodeposition and the cathode assembled from the crude material without adding any binder or conductive species exhibited a specific capacity of approximately 300 mA h g^{-1}.[217] Despite these good results obtained from amorphous MnO_2, amorphous MnO_2 often showed a quick fading rate during repeated cycles. Although the exact failure mechanism is not clear yet, the instability of the amorphous structure and the conglomeration of the small particles during cycling could be the possible reasons. There are also corresponding efforts to solve the problem by doping other elements such as Na,[218] Cu[219] or Bi[220] to achieve improved cycling performance by stabilizing the local structure.

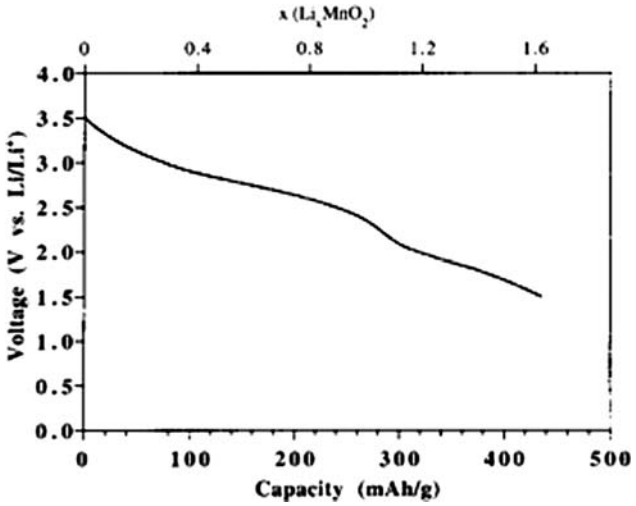

Fig. 11 Variation of electrode potential with lithium ion content upon insertion into the oxide at a current density of 20 μA cm^{-2}.[215]

Amorphous intercalation compounds often exhibit sloping charge/discharge curves instead of possessing a well-defined plateau which was characteristic of well crystallized intercalation compound.[221] As a result, the average intercalation voltage was lower. The energy density of a lithium ion battery is a product of capacity C and voltage V. The amorphous intercalation electrodes sacrifice the level of V for higher capacity C. In the case of amorphous MnO_2 whose intercalation discharge curve is shown in Fig. 11,[215] the sloping discharge curve possessed an average voltage of *ca.* 2.5 V, lower than 3 V reported from well-crystallized MnO_2,[124] however, the high capacity of more than 400 mA h g^{-1} was more than double the capacity of the well crystallized counterpart and the energy density was thus increased. In general, when calculating the energy density of amorphous intercalation electrodes, both voltage drop and capacity increase need to be considered.

4.2 Crystallinity effect on intercalation of capability of TiO_2 nanotube arrays

After the discussion on the relationships between the lithium ion intercalation and the surface defects and amorphortized phases, one would reasonably wonder about the impact of perfection of crystal structure on the lithium ion intercalation properties. The lithium ion intercalation capacity and cyclic stability of TiO_2 nanotube arrays with different crystallinity have been studied. Pristine TiO_2 nanotube arrays fabricated by anodic oxidation were amorphous and the samples annealed at 400 °C for 3 h in nitrogen exhibited dominant anatase phase.[210] Lithium ion intercalation measurements were carried out on these two samples together with two others treated at 300 °C and 500 °C and the cyclic performance was compared as shown in Fig. 12. It was found that the amorphous array possessed a high initial

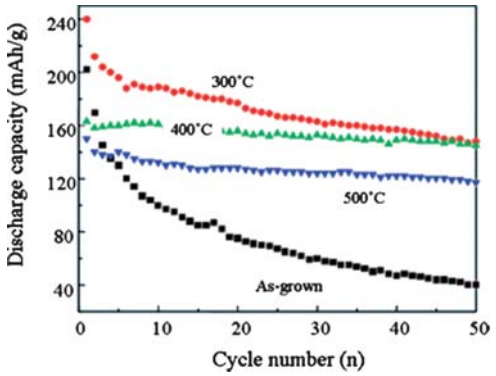

Fig. 12 Li^+-ion intercalation discharge capacity of amorphous as-grown TiO_2 nanotube arrays and anatase TiO_2 nanotube arrays annealed at 300, 400, and 500 °C in nitrogen for 3 h as a function of cyclic number. The measurements were carried out in a potential window between −0.6 and −2.1 V *vs.* Ag/AgCl as a reference electrode at a current density of 320 mAg^{-1}.[210]

capacity of (202 mA h g^{-1}). However, the cyclic stability was very poor and after 50 cycles the capacity was merely 40 mA h g^{-1}. Upon crystallization, the cyclic stability was obviously improved. 300 °C annealed arrays started with a high capacity of 240 mA h g^{-1} and ended up at 148 mA h g^{-1}. Well crystallized 400 °C arrays had a lower initial capacity of 163 mA h g^{-1} but the capacity after 50 cycles was still as high as 145 mA h g^{-1}. Higher temperature annealed arrays exhibited similar stability but the absolute capacity further decreased. Amorphous TiO_2 nanotube arrays might have higher capacities because of the more available sites to lithium ion intercalation (due to the defected and the disordered structure), However, because of the lithium diffusion limitation and the poor electronic conductivity, the cyclic stability of amorphous arrays was severely reduced as compared to well crystallized counterparts.

There were also some reports of composites having more amorphous structure than single oxides with good crystallinity due to the crystallization competition between oxides. TiO_2 were added to V_2O_5 following the sol–gel route.[222] While pure V_2O_5 xerogel exhibited typical hydrated V_2O_5 peaks, after introducing TiO_2, no noticeable peaks were found and this suggested the amorphous state of the composites. Even after annealing at 500 °C for 1 h, the crystallinity was still poor. The intercalation capability of the amorphous composites were measured and compared with pure V_2O_5 film; it was found that all the composites films with different composition ratios exhibited a higher capacity and the composition of V/Ti = 80/20 exhibited a very high initial capacity of more than 400 mA h g^{-1}. An *et al.* added amorphous NiO_2 nanoparticles to a mixture of TiO_2-B and anatase TiO_2 nanotubes and both the cyclic stability and capacities at high current densities were improved.[223]

Silicon anode was another good system to demonstrate the advantage of amorphous electrodes. While crystalline silicon often suffers severe volume change during lithium ion intercalation/de-intercalation and possessed low cyclic stability,[224] amorphous silicon showed a far less severe problem and could deliver stable high capacity over hundreds of cycles.[225] Amorphous silicon thin film prepared by DC magnetron sputtering of silicon on stainless steel substrates showed a good performance with a stable capacity of about 3000 mA h g^{-1} and a relatively low irreversible capacity.[226] Similar stability of high capacity was also reported on amorphous Si film made by pulsed laser deposition.[227,228]

It is somewhat arbitrary to conclude that amorphous structures deliver a higher capacity than well crystallized structure, or the opposite, because the situation varies depending on the intercalation compounds, *e.g.* the different story of TiO_2 and V_2O_5 as discussed above. However, while the lithium ion storage capability of well crystallized structures is already well known and subject to little chance of ground-breaking improvement, appropriate manipulation of amorphous or low-crystallinity structures could be a good route to circumvent some of the limitations of the rigid structure and achieve significant advances.

5. Direct fabrication of nanostructured film electrodes

5.1 Development of binder- and carbon-free film electrodes

The electrodes for lithium-ion batteries are typically fabricated by mixing electroactive materials with conductive additive (typically 10–15% acetylene black in weight or volume) and binders (typically poly(vinylidene fluoride) 5%–10% in weight or volume) with *n*-methyl-2-pyrrolidone NMP as solvent to make a slurry, and then tape-casting into a film electrode. The as-obtained film electrode is then subjected to drying at 120 °C for 12 h or so.[229–231] Such fabrication methods have been widely used in both industry and research laboratories and proved to be very successful. However, the addition of conductive additive and binder introduces extra processing steps and also compromises the amount of electroactive materials in electrodes.[232,233] The use of binder incurs more problems related with side reactions during the working cycles of electrodes.[234,235] Conventional admixing method may not be the best for obtaining the nanostructured electrodes. Direct fabrication of nanostructured film electrodes from solution chemical methods may offer some advantages. One justification for the introduction of conductive additive is for the favor of rate capability.[236,237] However, when the film electrodes are appropriately designed and fabricated, *e.g.* nanostructure and surface defective film, the surface charge transfer and diffusion process could be improved and there would be no need to add conductive additive and binders.

Preparation of binderless and carbon-free thin film electrodes were reported by several groups utilizing radio frequency (rf) magnetron sputtering,[238,239] pulsed laser deposition (PLD),[240,241] electrostatic spray deposition (ESD),[242,243] sol–gel spin coating[244,245] to directly deposit electroactive materials onto conductive substrates. These thin film electrodes without any additive exhibited comparable electrochemical performance to binder and carbon-added electrodes. In our experiments, we fabricated nanostructured thin film electrodes by sol–gel derived coating and electrodeposition. To improve the rate capability of thin film electrodes, we also modified the surface chemistry of electrodes and obtained good storage capacities under large charge/discharge current density.

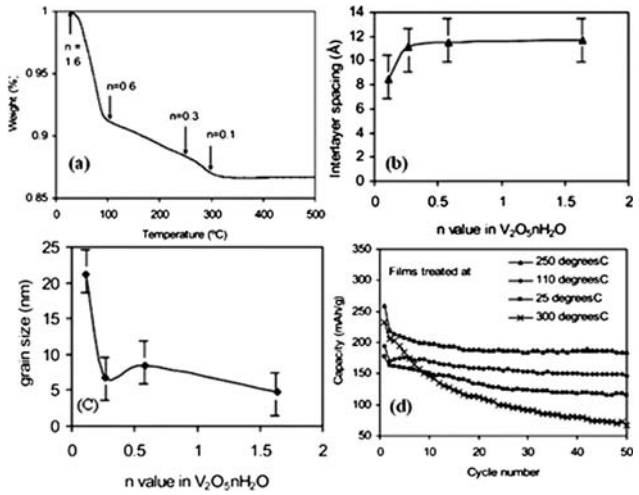

Fig. 13 (a) TGA curve for $V_2O_5 \cdot nH_2O$ xerogels, (b) dependence of interlayer spacing on the n value in $V_2O_5 \cdot nH_2O$, (c) dependence of grain size on the n value in $V_2O_5 \cdot nH_2O$ and (d) cycling performance at a current density of 100 μA cm^{-2} for $V_2O_5 \cdot nH_2O$ films obtained at 25, 110, 250 and 300 °C. The voltage ranges from 0.4 to −1.6 V *vs.* Ag/Ag$^+$.[205]

5.2 Sol–gel derived films by drop coating or electrophoretic deposition

V_2O_5 sol–gel derived films were made by drop casting vanadium pentoxide sol onto conductive ITO glass.[205] V_2O_5 coated ITO glass was used as the working electrode for the lithium ion intercalation study without any carbon or binder additive. The as-fabricated film without any post treatment was confirmed to be $V_2O_5 \cdot 1.6H_2O$ and after thermal treatment of increasing temperatures, the xerogel film started to lose crystal water (Fig. 13a) and underwent crystallinity change. The crystallinity including crystal structure, interlayer distance and grain size was dependent on the annealing temperature as confirmed by XRD study. While the interlayer distance remained ~11 Å when the annealing temperature was below 250 °C and crystal water content $n \geq 0.3$, further increase of annealing temperature, *i.e.* 300 and 330 °C induced sharp shrinkage of interlayer distance to about 8 Å (Fig. 13b). In addition, well crystallized orthorhombic V_2O_5 phase started to form and the grain size became much larger (Fig. 13c). The lithium ion intercalation capacities in long cycles of films treated under different temperatures were measured and the well crystallized V_2O_5 showed quick capacity fading over all the cycles while the less crystallized 250 °C annealed film exhibited a high initial capacity of ~275 mA h g^{-1} and stabilized at 185 mA h g^{-1} after 50 cycles (Fig. 13d).

V_2O_5 sol–gel derived film could also be synthesized through electrophoretic deposition. Electrophoretic deposition refers to the migration of colloidal particles suspended in a liquid medium under the influence of an electric field and deposition onto an electrode. It is a useful technique to deposit polycrystalline films with controlled crystalline texture and good porosity. In addition, it is simple and low cost with film thickness controllable by adjusting deposition conditions which are favorable for energy storage device electrodes. Zhitomirsky's group has adopted electrophoretic deposition method to fabricate manganese oxide or manganese oxide–carbon nanotube composites films used as electrochemical supercapacitors with capacitances of 150 Fg^{-1} for pure manganese oxide and 650 F g^{-1} for composites being obtained.[246,247] As a lithium ion battery electrode, V_2O_5 film could also be prepared by electrophoretic deposition from V_2O_5 sol using an anodic voltage 5 V followed by film calcination in air at 500 °C for 1 h.[248] The resultant film exhibited an initial capacity of 250 mA h g^{-1} and increased to 310 mA h g^{-1} after 50 cycles in a potential window between 0.4 and −1.6 V.

5.3 Mesoporous MnO_2 electrodes

Other solution-based methods have also been developed or used for the direct fabrication of porous nanostructure electrode films for lithium ion intercalation. For example, hierarchically structured mesoporous manganese dioxide nanowall arrays on cathodic substrates deposited by means of water electrolysis induced precipitation is an example for template-less fabrication of nanostructured electrodes.[249,250] The formation of the mesoporous nanowall arrays was the result of water-electrolysis induced precipitation, as depicted in Fig. 14a: during the precipitation, the metal substrate surface consisted of two kinds of sites; one was where the nanoparticles of manganese hydroxide were precipitated and the other was where hydrogen gas bubbling occurred (no precipitation). This discontinuous precipitation on the substrate generated the macroporous nanowall arrays. In addition, in every precipitation cluster, in the space between neighboring nanoparticles were mesopores as

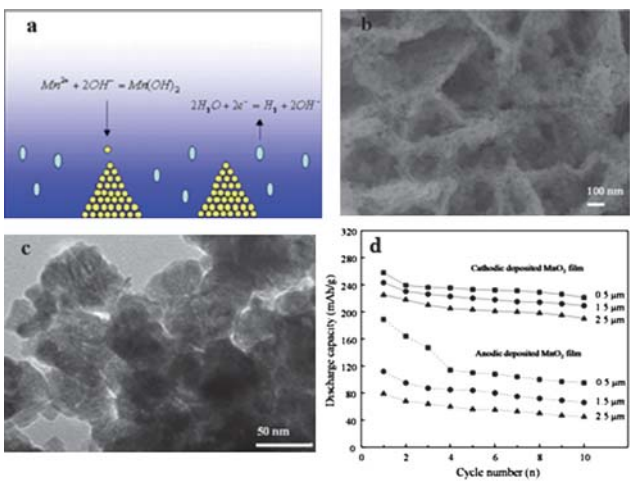

Fig. 14 (a) Scheme showing the proposed growth mechanisms of hierarchically structured manganese hydroxide nanowall arrays on cathodes due to the increased pH value resulting from water electrolysis (blue area stands for high pH): precipitation of manganese hydroxide nanoparticles from the electrolyte accompanied with the release of hydrogen gas bubbles from the cathode surface, (b) SEM image of the hierarchically structured nanowall arrays reflecting the structure proposed in the growth mechanism scheme, (c) TEM image of stacked nanoparticles in a nanowall with voids (pores) and (d) comparison of discharge capacities of anodic deposited manganese dioxide and cathodic deposited manganese dioxide in the first 10 cycles. The measurements were carried out between 0.4 V and −1.4 V *vs.* Ag/AgCl at a current density of 30 mA g^{-1}.[249]

found by TEM, and the nitrogen isotherm study revealed a large surface area $\sim 96\ m^2\ g^{-1}$ and a pore size of ~4.6 nm. In Fig. 14b and 14c, SEM and TEM images clearly indicated that the deposited hierarchical nanowall arrays were formed by closely stacked spherical nanoparticles with sizes around 50 nm. During the deposition, water electrolysis provided not only OH^- which bonded with Mn^{2+} to precipitate manganese hydroxide nanoparticles but also generated H_2 gas bubbles acting so as to prevent continuous precipitation on the whole substrate, thus producing the macropores of the nanowall arrays. Similar macroporous and mesoporous hierarchical structure was also found in cathodically deposited $Co(OH)_2$.[251]

The electrochemical properties of the as-fabricated nanowall arrays were directly measured on the platinum substrate without any electrode refinement and compared with an anodic oxidized MnO_2 film. In the lithium-ion intercalation test, both the cathodic and anodic MnO_2 were measured for different deposition thicknesses, *i.e.* 0.5, 1.5 and 2.5 μm and the long time cyclic performance of different thicknesses was compared in Fig. 14d. It was obvious that cathodic deposited manganese dioxide possessed a higher discharge capacity and better stability over anodic deposited manganese dioxide for each thickness. For the mesoporous nanowall arrays, when the film thickness was 0.5 μm, the initial capacity was as high as 256 mA h g^{-1} and after the thickness was increased to 2.5 μm, the initial capacity was still as high as 230 mA h g^{-1}.

The above comparison clearly revealed that the cathodically deposited manganese dioxide films possessed a favorable hierarchically mesoporous structure with higher discharge capacities and better cycle stability than anodically deposited manganese dioxide. The cyclic stability improvement could be attributed to the mesoporous structure of cathodic deposited manganese dioxide nanowall arrays. As to the high discharge capacities at large deposition thickness, the macrostructure should be the key point. Besides the large surface area and shorter diffusion path provided for lithium-ion reaction, like tube arrays, this honeycomb macroporous structure facilitated the penetration of electrolyte to the bottom of the array even when thickness was large, thus minimizing the adverse effect of large deposition thickness, *i.e.* difficulty of electrolyte penetration. A similar phenomenon was also found when making a comparison of the thickness effect on vanadium oxide with and without macroporous structures.[252,253] There are also other reports of porous thin film electrodes made by direct electrostatic spray deposition without binder and carbon additive introduction that exhibited excellent electrochemical performance, *e.g.* porous Fe_2O_3 film,[254] porous $Li_4Ti_5O_{12}$[255] and porous NiO.[256]

Acidic anodization has been yet another method to fabricate electrode films for lithium ion intercalation. TiO_2 nanotube arrays could be fabricated by anodization of Ti foil in a two-electrode electrochemical cell with platinum foil as a cathode at a constant potential at room temperature.[257,258] Polished Ti foil was anodized in different types of electrolytes for 1 h to form nanotube arrays on Ti substrate. The nanotube diameters and length could be controlled by changing the anodization voltage and time. The as-fabricated TiO_2 nanotube arrays exhibited excellent intercalation properties after appropriate heat treatment in nitrogen or carbon monoxide gas as discussed in section 3.2 and 4.2.

6. Concluding remarks

No era in human history has witnessed as fast a boom of the energy industry as the past decade. The invention of rechargeable lithium ion battery has actively changed the functionality of the modern life style by providing the uninterrupted power for electronic devices on the constant move such as cellular phones and laptops. Various kinds of intercalation electrodes have been studied and reported to have achieved high specific energy and high specific power as well as long lifetime. However, what was growing faster than the development of lithium ion battery was the human demand and social expectation supported by the rapid advancement of electronics. In addition, the increasing public awareness on environmental issues has been putting more pressures on clean sustainable energy including lithium ion batteries. In contrast to the ever-growing demands, the candidate pool of intercalation electrodes is limited. The introduction of nanostructures has achieved a huge success in the lithium ion battery field, as it did in many other fields. The essential contribution of nanostructure to the improvement of the intercalation capability lies not only in the increased specific surface area for interfacial Faradaic reactions and the reduced and favorable mass and charge diffusion path for lithium ions and electrons, but also in the modification of the surface thermodynamics and kinetics which facilitates the phase transition. The nanostructured electrodes have demonstrated their capabilities to accommodate an amount of lithium ions higher than that of their counterpart electrodes with micrometre-sized structure (referred to as bulk materials). Recently the thermodynamically non-equilibrium effects of nanostructured electrodes are being increasingly recognized. The presence of surface defects has also demonstrated to modify the surface thermodynamics and facilitate the phase transition boundary. The amorphous state could possibly store more lithium ions because of its more open structure; similar results have been reported in electrodes with poor crystallinity. Materials possessing nanostructures and surface and bulk defects and in poor crystallinity or amorphous state all lie away the from the equilibrium state. Such electrodes away from equilibrium state have demonstrated favorable lithium ion intercalation properties. The contribution of non-equilibrium state lies in three aspects: (1) enhancing the storage capacity by shifting the phase transition boundary; (2) improving the rate capability by introducing a fast mass and charge transport path; and (3) allowing longer cyclic stability by permitting more freedom for volume change accompanied by lithium ion intercalation and de-intercalation. The drawbacks of the electrodes away from equilibrium state is their chemical and structure stability; surface coating and passivation have been explored and studied to counter this challenge. The development of binderless and carbon-free film electrodes with appropriately designed nanostructures would be another exciting research direction, as the conventional electrode fabrication methods are not suitable for the retention of nanostructures. Film electrodes have the advantages of easy fabrication and high energy storage density but suffer from low rate capability because of absence of conductive species, however, nanostructured film electrodes could achieve comparable or higher rate capability when the appropriately designed nano and microstructures and surface chemistry are applied.

Acknowledgements

D. W. L would like to acknowledge the graduate fellowship from the University of Washington Center for Nanotechnology (CNT). This work is also supported by NSF (DMI-0455994 and DMR-0605159), AFOSR (MURI, FA955006-1-0326), NCNT (Korea), WTC, PNNL and EnerG2.

References

1 M. Z. Jacobson, *Energy Environ. Sci.*, 2009, **2**, 148.
2 N. S. Lewis and D. G. Nocera, *Proc. Natl. Acad. Sci. U. S. A.*, 2006, **103**, 15731.
3 P. Xie and R. B. Zhang, *J. Mater. Chem.*, 2005, **15**, 2529.
4 G. Petrone, G. Spagnuolo, R. Teodorescu, M. Veerachary and M. Vitelli, *IEEE Trans. Ind. Electron.*, 2008, **55**, 2569.
5 A. P. Kulkarni, C. J. Tonzola, A. Babel and S. A. Jenekhe, *Chem. Mater.*, 2004, **16**, 4556.
6 K. M. Coakley and M. D. McGehee, *Chem. Mater.*, 2004, **16**, 4533.
7 J. E. Fernandez, *Science*, 2007, **315**, 1807.
8 M. S. Dresselhaus, G. Chen, M. Y. Tang, R. G. Yang, H. Lee, D. Z. Wang, Z. F. Ren and J. P. Fleurial, *Adv. Mater.*, 2007, **19**, 1043.
9 L. E. Bell, *Science*, 2008, **321**, 1457.
10 I. B. Fridleifsson, *Renewable Sustainable Energy Rev.*, 2001, **5**, 299.
11 M. Asif and T. Muneer, *Renewable Sustainable Energy Rev.*, 2007, **11**, 1388.
12 Q. F. Zhang, C. S. Dandeneau, X. Y. Zhou and G. Z. Cao, *Adv. Mater.*, 2009, **21**, 4087.
13 M. Granovskii, I. Dincer and M. A. Rosen, *J. Power Sources*, 2007, **167**, 461.
14 D. P. Birnie III, *J. Power Sources*, 2009, **186**, 539.
15 V. Ananthachar and J. J. Duffy, *Sol. Energy*, 2005, **78**, 687.
16 J. Linnemann and R. Steinberger-Wilckens, *Int. J. Hydrogen Energy*, 2007, **32**, 1492.
17 Y. Qin, X. D. Wang and Z. L. Wang, *Nature*, 2008, **451**, 809.
18 R. Yevich and J. A. Logan, *Global Biogeochem. Cycles*, 2003, **17**, 1095.
19 R. Luque, L. Herrero-Davila, J. M. Campelo, J. H. Clark, J. M. Hidalgo, D. Luna, J. M. Marinas and A. A. Romero, *Energy Environ. Sci.*, 2008, **1**, 542.
20 R. H. Crabtree, *Energy Environ. Sci.*, 2008, **1**, 134.
21 A. Feaver, S. Sepehri, P. Shamberger, A. Stowe, T. Autrey and G. Z. Cao, *J. Phys. Chem. B*, 2007, **111**, 7469.
22 B. Batalla Garcia, A. M. Feaver, Q. F. Zhang, R. D. Champion, G. Z. Cao, T. T. Fister, K. P. Nagle and G. T. Seidler, *J. Appl. Phys.*, 2008, **104**, 014305.
23 P. Simon and Y. Gogotsi, *Nat. Mater.*, 2008, **7**, 845.
24 M. S. Whittingham, *Chem. Rev.*, 2004, **104**, 4271.
25 R. J. Brodd, K. R. Bullock, R. A. Leising, R. L. Middaugh, J. R. Miller and E. Takeuchi, *J. Electrochem. Soc.*, 2004, **151**, K1.
26 W. H. Meyer, *Adv. Mater.*, 1998, **10**, 439.
27 G. Y. Adachi, N. Imanaka and H. Aono, *Adv. Mater.*, 1996, **8**, 127.
28 Y. Wang and G. Z. Cao, *Chem. Mater.*, 2006, **18**, 2787.
29 M. Armand and J. M. Tarascon, *Nature*, 2008, **451**, 652.
30 S. F. J. Flipsen, *J. Power Sources*, 2006, **162**, 927.
31 J. Mader, *IEEE AES Syst. Mag.*, 1996, **11**, 17.
32 M. Winter and R. J. Brodd, *Chem. Rev.*, 2004, **104**, 4245.
33 J. M. Tarascon and D. Guyomard, *Electrochim. Acta*, 1993, **38**, 1221.
34 P. Arora, R. E. White and M. Doyle, *J. Electrochem. Soc.*, 1998, **145**, 3647.
35 H. Li, Z. X. Wang, L. Q. Chen and X. J. Huang, *Adv. Mater.*, DOI: 10.1002/adma.200901710.
36 X. W. Lou, Y. Wang, C. L. Yuan, J. Y. Lee and L. A. Archer, *Adv. Mater.*, 2006, **18**, 2325.
37 F. M. Zhan, B. Y. Geng and Y. J. Guo, *Chem.–Eur. J.*, 2009, **15**, 6169.
38 M. Winter, J. O. Besenhard, M. E. Spahr and P. Novak, *Adv. Mater.*, 1998, **10**, 725.
39 A. S. Aricò, P. G. Bruce, B. Scrosati, J. M. Tarascon and W. Van Schalkwijk, *Nat. Mater.*, 2005, **4**, 366.
40 M. J. Zou, M. Yoshio, S. Gopukumar and J. I. Yamaki, *Chem. Mater.*, 2003, **15**, 4699.
41 P. Strobel, S. Rohs and F. Le Cras, *J. Mater. Chem.*, 1996, **6**, 1591.
42 J. B. Goodenough, *J. Power Sources*, 2007, **174**, 996.
43 S. Ahn, Y. Kim, K. J. Kim, T. H. Kim, H. Lee and M. H. Kim, *J. Power Sources*, 1999, **81–82**, 896.
44 L. J. Fu, T. Zhang, Q. Cao, H. P. Zhang and Y. P. Wu, *Electrochem. Commun.*, 2007, **9**, 2140.
45 J. Reed and G. Ceder, *Chem. Rev.*, 2004, **104**, 4513.
46 M. Nishizawa, H. Koshika and I. Uchida, *J. Phys. Chem. B*, 1999, **103**, 192.
47 F. S. Ke, L. Huang, H. H. Jiang, H. B. Wei, F. Z. Yang and S. G. Sun, *Electrochem. Commun.*, 2007, **9**, 228.
48 J. W. Long, B. Dunn, D. R. Rolison and H. S. White, *Chem. Rev.*, 2004, **104**, 4463.
49 Y. X. Gu, D. R. Chen and M. L. Jiao, *J. Phys. Chem. B*, 2005, **109**, 17901.
50 K. H. Reiman, K. M. Brace, T. J. Gordon-Smith, I. Nandhakumar, G. S. Attard and J. R. Owen, *Electrochem. Commun.*, 2006, **8**, 517.
51 J. Hu, H. Li, X. J. Huang and L. Q. Chen, *Solid State Ionics*, 2006, **177**, 2791.
52 H. J. Liu, S. H. Bo, W. J. Cui, F. Li, C. X. Wang and Y. Y. Xia, *Electrochim. Acta*, 2008, **53**, 6497.
53 L. J. Fu, H. Liu, C. Li, Y. P. Wu, E. Rahm, R. Holze and H. Q. Wu, *Solid State Ionics*, 2006, **8**, 113.
54 G. A. Wiegers, *Prog. Solid State Chem.*, 1996, **24**, 1.
55 K. Ui, S. Y. Funo, H. Nagase, Y. Idemoto and N. Koura, *Electrochemistry*, 2006, **74**, 474.
56 L. Ji and X. Zhang, *Electrochem. Commun.*, 2009, **11**, 1146.
57 C. C. Li, J. T. Lee and X. W. Peng, *J. Electrochem. Soc.*, 2006, **153**, A809.
58 N. Imanishi, K. Kanamura and Z. Takehara, *J. Electrochem. Soc.*, 1992, **139**, 2082.
59 A. Eftekhari, *J. Power Sources*, 2003, **124**, 182.
60 Q. Y. Li, S. J. Hu, H. Q. Wang, F. P. Wang, X. X. Zhong and X. Y. Wang, *Electrochim. Acta*, 2009, **54**, 5884.
61 B. J. Neudecker, R. A. Zuhr and J. B. Bates, *J. Power Sources*, 1999, **81**, 27.
62 J. Song, X. Yang, S. S. Zeng, M. Z. Cai, L. T. Zhang, Q. F. Dong, M. S. Zheng, S. T. Wu and Q. H. Wu, *J. Micromech. Microeng.*, 2009, **19**, 045004.
63 G. Z. Cao, *Nanostructures and Nanomaterials, Synthesis, Properties and Applications*, Imperial College Press, London, 2004.
64 A. Bachtold, P. Hadley, T. Nakanishi and C. Dekker, *Science*, 2001, **294**, 1317.
65 Y. Cui, Q. Wei, H. Park and C. M. Lieber, *Science*, 2001, **293**, 1289.
66 P. Xiao, D. W. Liu, B. B. Garcia, S. Sepehri, Y. H. Zhang and G. Z. Cao, *Sens. Actuators, B*, 2008, **134**, 367.
67 T. P. Chou, Q. F. Zhang, G. E. Fryxell and G. Z. Cao, *Adv. Mater.*, 2007, **19**, 2588.
68 Q. F. Zhang, T. P. Chou, B. Russo, S. A. Jenekhe and G. Z. Cao, *Angew. Chem., Int. Ed.*, 2008, **47**, 2402.
69 K. Takahashi, S. J. Limmer, Y. Wang and G. Z. Cao, *J. Phys. Chem. B*, 2004, **108**, 9795.
70 P. G. Bruce, *Solid State Ionics*, 2008, **179**, 752.
71 A. K. Padhi, K. S. Nanjundaswamy and J. B. Goodenough, *J. Electrochem. Soc.*, 1997, **144**, 1188.
72 K. Zaghib, A. Mauger, F. Gendron and C. M. Julien, *Chem. Mater.*, 2008, **20**, 462.
73 S. Y. Chung and Y. M. Chiang, *Electrochem. Solid-State Lett.*, 2003, **6**, A278.
74 P. S. Herle, B. Ellis, N. Coombs and L. F. Nazar, *Nat. Mater.*, 2004, **3**, 147.
75 Y. Xia, M. Yoshio and H. Noguchi, *Electrochim. Acta*, 2006, **52**, 240.
76 N. J. Yun, H. W. Ha, K. H. Jeong, H. Y. Park and K. Kim, *J. Power Sources*, 2001, **97–98**, 508.
77 A. Yamada, S. C. Chung and K. Hinokuma, *J. Electrochem. Soc.*, 2001, **148**, A224.
78 M. Takahashi, Sh. Tobishima, K. Takei and Y. Sakurai, *J. Power Sources*, 2001, **97–98**, 508–511.
79 N. Kosova and E. Devyatkina, *Solid State Ionics*, 2004, **172**, 181.
80 M. Higuchi, K. Katayama, Y. Azuma, M. Yukawa and M. Suhara, *J.Power Sources*, 2003, **119–121**, 258.
81 D. Jugovic and D. Uskokovic, *J. Power Sources*, 2009, **190**, 538.

82 J. J. Chen and M. S. Whittingham, *Electrochem. Commun.*, 2006, **8**, 855.
83 B. Ellis, W. H. Kan, W. R. M. Makahnouk and L. F. Nazar, *J. Mater. Chem.*, 2007, **17**, 3248.
84 H. Yang, X. L. Wu, M. H. Cao and Y. G. Guo, *J. Phys. Chem. C*, 2009, **113**, 3345.
85 N. Recham, L. Dupont, M. Courty, K. Djellab, D. Larcher, M. Armand and J. M. Tarascon, *Chem. Mater.*, 2009, **21**, 1096.
86 G. X. Wang, X. P. Shen and J. Yao, *J. Power Sources*, 2009, **189**, 543.
87 D. W. Choi and P. N. Kumta, *J. Power Sources*, 2007, **163**, 1064.
88 R. Dominko, M. Bele, J. M. Goupil, M. Gaberscek, D. Hanzel, I. Arcon and J. Jamnik, *Chem. Mater.*, 2007, **19**, 2960.
89 Y. Q. Wang, J. L. Wang, J. Yang and Y. N. Nuli, *Adv. Funct. Mater.*, 2006, **16**, 2135.
90 G. Meligrana, C. Gerbaldi, A. Tuel, S. Bodoardo and N. Penazzi, *J. Power Sources*, 2006, **160**, 516.
91 A. V. Murugan, T. Muraliganth and A. Manthiram, *J. Phys. Chem. C*, 2008, **112**, 14665.
92 R. Dominko, M. Bele, M. Gaberscek, M. Remskar, D. Hanzel, J. M. Goupil, S. Pejovnik and J. Jamnik, *J. Power Sources*, 2006, **153**, 274.
93 F. Yu, J. J. Zhang, Y. F. Yang and G. Z. Song, *J. Mater. Chem.*, 2009, **19**, 9121.
94 G. Arnold, J. Garche, R. Hemmer, S. Strobele, C. Vogler and M. Wohlfahrt-Mehrens, *J. Power Sources*, 2003, **119–121**, 247.
95 M. R. Yang, W. H. Ke and S. H. Wu, *J. Power Sources*, 2005, **146**, 539.
96 T. H. Cho and H. T. Chung, *J. Power Sources*, 2004, **133**, 272.
97 S. T. Myung, Sh. Komaba, N. Hirosaki, H. Yashiro and N. Kumagai, *Electrochim. Acta*, 2004, **49**, 4213.
98 S. Y. Yin, L. Song, X. Y. Wang, M. F. Zhang, K. L. Zhang and Y. X. Zhang, *Electrochim. Acta*, 2009, **54**, 5629.
99 D. Peramunage and K. M. Abraham, *J. Electrochem. Soc.*, 1998, **145**, 2609.
100 J. L. Allen, T. R. Jow and J. Wolfenstine, *J. Power Sources*, 2006, **159**, 1340.
101 A. Jaiswal, C. R. Horne, O. Chang, W. Zhang, W. Kong, E. Wang, T. Cherm and M. M. Doeff, *J. Electrochem. Soc.*, 2009, **156**, A1041.
102 H. W. Lu, W. Zeng, Y. S. Li and Z. W. Fu, *J. Power Sources*, 2007, **164**, 874.
103 J. Y. Kim and J. P. Cho, *Electrochem. Solid-State Lett.*, 2007, **10**, A81.
104 J. Gao, J. R. Ying, C. Y. Jiang and C. R. Wan, *J. Power Sources*, 2007, **166**, 255.
105 J. J. Huang and Z. Y. Jiang, *Electrochim. Acta*, 2008, **53**, 7756.
106 L. Cheng, J. Yan, G. N. Zhu, J. Y. Luo, C. X. Wang and Y. Y. Xia, *J. Mater. Chem.*, 2010, **20**, 595.
107 P. Heitjans and S. Indris, *J. Phys.: Condens. Matter*, 2003, **15**, R1257.
108 P. Poizot, S. Laruelle, S. Grugeon, L. Dupont and J. M. Tarascon, *Nature*, 2000, **407**, 496.
109 J. Schoonman, *Solid State Ionics*, 2000, **135**, 5.
110 J. Maier, *Nat. Mater.*, 2005, **4**, 805.
111 J. Maier, *Phys. Chem. Chem. Phys.*, 2009, **11**, 3011.
112 N. Meethong, H. Y. S. Huang, W. C. Carter and Y. M. Chiang, *Electrochem. Solid-State Lett.*, 2007, **10**, A134.
113 M. Wagemaker, W. J. H. Borghols, E. R. H. van Eck, A. P. M. Kentgens, G. J. Kearley and F. M. Mulder, *Chem.–Eur. J.*, 2007, **13**, 2023.
114 M. Wagemaker, W. J. H. Borghols and F. M. Mulder, *J. Am. Chem. Soc.*, 2007, **129**, 4323.
115 P. G. Bruce, B. Scrosati and J. M. Tarascon, *Angew. Chem., Int. Ed.*, 2008, **47**, 2930.
116 J. Yan, Z. Chen, J. Jiang, L. O. Tan and X. C. Zeng, *Adv. Mater.*, 2009, **21**, 314.
117 G. Z. Cao and D. W. Liu, *Adv. Colloid Interface Sci.*, 2008, **136**, 45.
118 I. Turyan and D. Mandler, *J. Am. Chem. Soc.*, 1998, **120**, 10733.
119 D. Q. Shi, J. P. Tu, Y. F. Yuan, H. M. Wu, Y. Li and X. B. Zhao, *Electrochem. Commun.*, 2006, **8**, 1610.
120 C. J. Patrissi and C. R. Martin, *J. Electrochem. Soc.*, 1999, **146**, 3176.
121 K. Takahashi, Y. Wang and G. Z. Cao, *J. Phys. Chem. B*, 2005, **109**, 48.
122 Y. Wang, K. Takahashi, H. M. Shang, K. H. Lee and G. Z. Cao, *J. Phys. Chem. B*, 2005, **109**, 3085.
123 Y. Wang, K. Takahashi, K. Lee and G. Z. Cao, *Adv. Funct. Mater.*, 2006, **16**, 1133.
124 M. Sugantha, P. A. Ramakrishnan, A. M. Hermann, C. P. Warmsingh and D. S. Ginley, *Int. J. Hydrogen Energy*, 2003, **28**, 597.
125 F. Y. Cheng, J. Z. Zhao, W. Song, C. S. Li, H. Ma, J. Chen and P. Shen, *Inorg. Chem.*, 2006, **45**, 2038.
126 T. X. T. Sayle, R. R. Maphanga, P. E. Ngoepe and D. C. Sayle, *J. Am. Chem. Soc.*, 2009, **131**, 6161.
127 A. R. Armstrong, G. Armstrong, J. Canales and P. G. Bruce, *Angew. Chem., Int. Ed.*, 2004, **43**, 2286.
128 A. R. Armstrong, G. Armstrong, J. Canales, R. Garcia and P. G. Bruce, *Adv. Mater.*, 2005, **17**, 862.
129 X. P. Gao, H. Y. Zhu, G. L. Pan, S. H. Ye, Y. Lan, F. Wu and D. Y. Song, *J. Phys. Chem. B*, 2004, **108**, 2868.
130 J. R. Li, Z. L. Tang and Z. T. Zhang, *Electrochem. Solid-State Lett.*, 1999, **3**, 316.
131 H. Zhang, G. R. Li, L. P. An, T. Y. Yan, X. P. Gao and H. Y. Zhu, *J. Phys. Chem. C*, 2007, **111**, 6143.
132 J. Y. Luo, J. J. Zhang and Y. Y. Xia, *Chem. Mater.*, 2006, **18**, 5618.
133 F. Cheng, Z. Tao, J. Liang and J. Chen, *Chem. Mater.*, 2008, **20**, 667.
134 A. S. Yu and R. Frech, *J. Electrochem. Soc.*, 2002, **149**, A99.
135 P. D. Yang, D. Zhao, D. I. Margolese, B. F. Chmelka and G. D. Stucky, *Nature*, 1998, **396**, 152.
136 L. Kavan, J. Rathousky, M. Gratzel, V. Shklover and A. Zukal, *J. Phys. Chem. B*, 2000, **104**, 12012.
137 D. Fattakhova-Rohlfing, M. Wark, T. Brezesinski, B. M. Smarsly and J. Rathousky, *Adv. Funct. Mater.*, 2007, **17**, 123.
138 P. Kubiak, J. Geserick, N. Husing and M. Wohlfahrt-Mehrens, *J. Power Sources*, 2008, **175**, 510.
139 X. W. Lou and L. A. Archer, *Adv. Mater.*, 2008, **20**, 1853.
140 P. Liu, S. H. Lee, C. E. Tracy, Y. F. Yan and J. A. Turner, *Adv. Mater.*, 2002, **14**, 27.
141 S. Lim, C. S. Yoon and J. Cho, *Chem. Mater.*, 2008, **20**, 4560.
142 F. Jiao and P. G. Bruce, *Adv. Mater.*, 2007, **19**, 657.
143 F. Jiao, J. L. Bao, A. H. Hill and P. G. Bruce, *Angew. Chem., Int. Ed.*, 2008, **47**, 9711.
144 A. K. Sinha, K. Suzuki, M. Takahara, H. Azuma, T. Nonaka and K. Fukumoto, *Angew. Chem., Int. Ed.*, 2007, **46**, 2891.
145 X. M. Ni, Y. F. Zhang, D. Y. Tian, H. G. Zheng and X. W. Wang, *J. Cryst. Growth*, 2007, **306**, 418.
146 P. Liu, S. H. Lee, C. E. Tracy, J. A. Turner, J. R. Pitts and S. K. Deb, *Solid State Ionics*, 2003, **165**, 223.
147 B. V. Ratnakumar, M. C. Smart and S. Surampudi, *J. Power Sources*, 2001, **97–98**, 137.
148 S. S. Zhang, K. Xu and T. R. Jow, *Electrochem. Solid-State Lett.*, 2002, **5**, A92.
149 F. Beguin, F. Chevallier, C. Vix-Guterl, S. Saadallah, V. Bertagna, J. N. Rouzaud and E. Frackowiak, *Carbon*, 2005, **43**, 2160.
150 J. Yan, B. J. Xia, Y. C. Su, X. Z. Zhou, J. Zhang and X. G. Zhang, *Electrochim. Acta*, 2008, **53**, 7069.
151 A. Lewandowski and A. Swiderska-Mocek, *J. Power Sources*, 2009, **194**, 601.
152 S. S. Zhang, *J. Power Sources*, 2006, **162**, 1379.
153 M. S. Wu, P. C. J. Chiang and J. C. Lin, *J. Electrochem. Soc.*, 2005, **152**, A1041.
154 T. Yoshida, M. Takahashi, S. Morikawa, C. Ihara, H. Katsukawa, T. Shiratsuchi and J. I. Yamaki, *J. Electrochem. Soc.*, 2006, **153**, A576.
155 K. Edström, A. M. Andersson, A. Bishop, L. Fransson, J. Lindgren and A. Hussenius, *J. Power Sources*, 2001, **97–98**, 87.
156 M. Itagaki, S. Yotsuda, N. Kobari, K. Watanabe, S. Kinoshita and M. Ue, *Electrochim. Acta*, 2006, **51**, 1629.
157 Y. S. Park and S. M. Lee, *Electrochim. Acta*, 2009, **54**, 3339.
158 M. Jo, Y. S. Hong, J. Choo and J. Cho, *J. Electrochem. Soc.*, 2009, **156**, A430.
159 J. L. Lei, L. J. Li, R. Kostecki, R. Muller and F. Mclarnon, *J. Electrochem. Soc.*, 2005, **152**, A774.
160 L. Yang, M. Takahashi and B. F. Wang, *Electrochim. Acta*, 2006, **51**, 3228.
161 D. H. Jang, Y. J. Shin and S. M. Oh, *J. Electrochem. Soc.*, 1996, **143**, 2204.
162 T. F. Yi, Y. R. Zhu, X. D. Zhu, J. Shu, C. B. Yue and A. N. Zhou, *Ionics*, 2009, **15**, 779.

163 S. H. Ye, J. Y. Lv, X. P. Gao, F. Wu and D. Y. Song, *Electrochim Acta*, 2004, **49**, 1623.
164 D. Aurbach, M. D. Levi, E. Levi, H. Teller, B. Markovsky, G. Salitra, U. Heider and L. Heider, *J. Electrochem. Soc.*, 1998, **145**, 3024.
165 C. L. Olson and I. Ballard, *J. Phys. Chem. B*, 2006, **110**, 1828.
166 Y. Yang, C. Xie, R. Ruffo, H. L. Peng, D. K. Kim and Y. Cui, *Nano Lett.*, 2009, **9**, 4109.
167 N. A. Chernova, M. Roppolo, A. C. Dillon and M. S. Whittingham, *J. Mater. Chem.*, 2009, **19**, 2526.
168 D. C. Li, Y. Sasaki, K. Kobayakawa and Y. Sato, *Electrochim. Acta*, 2006, **51**, 3809.
169 C. L. Tan, J. J. Zhou, W. S. Li, X. H. Hou, D. S. Lv, M. Q. Xu and Q. M. Huang, *J. Power Sources*, 2008, **184**, 408.
170 G. T. K. Fey, J. G. Chen and T. P. Kumar, *J. Power Sources*, 2005, **146**, 250.
171 B. Kim, C. Kim, T. G. Kim, D. Ahn and B. Park, *J. Electrochem. Soc.*, 2006, **153**, A1773.
172 H. W. Ha, N. J. Yun, M. H. Kim, M. H. Woo and K. Kim, *Electrochim. Acta*, 2006, **51**, 3297.
173 Z. R. Zhang, Z. L. Gong and Y. Yang, *J. Phys. Chem. B*, 2004, **108**, 17546.
174 N. Ohta, K. Takada, L. Q. Zhang, R. Z. Ma, M. Osada and T. Sasaki, *Adv. Mater.*, 2006, **18**, 2226.
175 N. V. Kosova and E. T. Devyatkina, *J. Power Sources*, 2007, **174**, 959.
176 G. T. K. Fey, C. Z. Lu, T. P. Kumar and Y. C. Chang, *Surf. Coat. Technol.*, 2005, **199**, 22.
177 M. Kaneko, M. Nakayama, Y. Wakizaka, K. Kanamura and M. Wakihara, *Electrochim. Acta*, 2008, **53**, 8196.
178 Y. Shao-horn, S. A. Hackney, A. J. Kahaina, K. D. Kepler, E. Skinner, J. T. Vaughey and M. M. Thackeray, *J. Power Sources*, 1999, **81–82**, 496.
179 K. M. Shaju and P. G. Bruce, *Chem. Mater.*, 2008, **20**, 5557.
180 G. Amatucci, A. Du Pasquier, A. Blyr, T. Zheng and J. M. Tarascon, *Electrochim. Acta*, 1999, **45**, 255.
181 Z. X. Yang, W. S. Yang, D. G. Evans, Y. Y. Zhao and X. Wei, *J. Power Sources*, 2009, **189**, 1147.
182 A. M. Kannan and A. Manthiram, *Electrochem. Solid-State Lett.*, 2002, **5**, A167.
183 J. Tu, X. B. Zhao, G. S. Cao, D. G. Zhuang, T. J. Zhu and J. P. Tu, *Electrochim. Acta*, 2006, **51**, 6456.
184 A. Eftekhari, *Solid State Ionics*, 2004, **167**, 237.
185 T. Okumura, T. Fukutsuka, Y. Uchimoto, K. Amezawa and S. Kobayashi, *J. Power Sources*, 2009, **189**, 471.
186 J. Han, S. Myung and Y. Sun, *J. Electrochem. Soc.*, 2006, **153**, A1290.
187 M. M. Thackeray, C. S. Johnson, J. S. Kim, K. C. Lauzze, J. T. Vaughey, N. Dietz, D. Abraham, S. A. Hackney, W. Zeltner and M. A. Anderson, *Electrochem. Commun.*, 2003, **5**, 752.
188 S. Y. Chung, J. T. Bloking and Y. M. Chiang, *Nat. Mater.*, 2002, **1**, 123.
189 S. F. Yang, Y. N. Song, K. Ngala, P. Y. Zavalij and M. S. Whittingham, *J. Power Sources*, 2003, **119–121**, 239.
190 N. Ravet, J. B. Goodenough, S. Besner, M. Simoneau, P. Hovington and M. Armand, *Electrochem. Soc. Abstr.*, 1999, **99–2**, 172.
191 I. Belharouak, C. Johnson and K. Amine, *Electrochem. Commun.*, 2005, **7**, 983.
192 F. Croce, A. D. Epifanio, J. Hassoun, A. Deptula, T. Olczac and B. Scrosati, *Electrochem. Solid-State Lett.*, 2002, **5**, A47.
193 J. Morales, R. Trocoli, E. Rodriguez-Castellon, S. Franger and J. Santos-Pena, *J. Electroanal. Chem.*, 2009, **631**, 29.
194 Y. S. Hu, Y. G. Guo, R. Dominko, M. Gaberscek, J. Jamnik and J. Maier, *Adv. Mater.*, 2007, **19**, 1963.
195 K. Saravanan, M. V. Reddy, P. Balaya, H. Gong, B. V. R. Chowdari and J. J. Vittal, *J. Mater. Chem.*, 2009, **19**, 605.
196 A. Odani, V. G. Pol, S. V. Pol, M. Koltypin, A. Gedanken and D. Aurbach, *Adv. Mater.*, 2006, **18**, 1431.
197 B. Li. He, B. Dong and H. L. Li, *Electrochem. Commun.*, 2007, **9**, 425.
198 M. Mancini, P. Kubiak, J. Geserick, R. Marassi, N. Husing and M. Wohlfahrt-Mehrens, *J. Power Sources*, 2009, **189**, 585.
199 F. Tanguy, J. Gaubicher, A. C. Gaillot, D. Guyomard and J. Pinson, *J. Mater. Chem.*, 2009, **19**, 4771.
200 D. R. Rolison and B. Dunn, *J. Mater. Chem.*, 2001, **11**, 963.
201 P. Xiao, B. B. Garcia, Q. Guo, D. W. Liu and G. Z. Cao, *Electrochem. Commun.*, 2007, **9**, 2441.
202 D. W. Liu, Y. H. Zhang, P. Xiao, B. B. Garcia, Q. F. Zhang, X. Y. Zhou, Y. H. Jeong and G. Z. Cao, *Electrochim. Acta*, 2009, **54**, 6816.
203 K. E. Swider-Lyons, C. T. Love and D. R. Rolison, *Solid State Ionics*, 2002, **152–153**, 99.
204 D. W. Liu, Y. Y. Liu, B. B. Garcia, Q. F. Zhang, A. Q. Pan, Y. H. Jeong and G. Z. Cao, *J. Mater. Chem.*, 2009, **19**, 8789.
205 Y. Wang, H. M. Shang, T. Chou and G. Z. Cao, *J. Phys. Chem. B*, 2005, **109**, 11361.
206 J. Cho, T. J. Kim and B. Park, *J. Electrochem. Soc.*, 2002, **149**, A288.
207 B. Kang and G. Ceder, *Nature*, 2009, **458**, 190.
208 S. Pyun and J. S. Bae, *J. Power Sources*, 1997, **68**, 669.
209 L. J. Fu, H. Liu, C. Li, Y. P. Wu, E. Rahm, R. Holze and H. Q. Wu, *Solid State Sci.*, 2006, **8**, 113.
210 D. W. Liu, P. Xiao, Y. H. Zhang, B. B. Garcia, Q. F. Zhang, Q. Guo, R. Champion and G. Z. Cao, *J. Phys. Chem. C*, 2008, **112**, 11175.
211 H. S. Jung, H. Shin, J. R. Kim, J. Y. Kim, K. S. Hong and J. K. Lee, *Langmuir*, 2004, **20**, 11732.
212 C. M. Julien, *Mater. Sci. Eng., R*, 2003, **40**, 47.
213 C. M. Park and H. J. Sohn, *Adv. Mater.*, 2010, **22**, 47.
214 M. S. Whittingham, R. S. Chianelli, A. J. Jacobson, in: D. W. Murphy, J. Broadhead, B. C. H. Steele (ed.), *Materials for Advanced Batteries*, Plenum Press, New York, 1980, p. 291.
215 J. J. Xu, A. J. Kinser, B. B. Owens and W. H. Smyrl, *Electrochem. Solid-State Lett.*, 1999, **1**, 1.
216 J. J. Xu and J. S. Yang, *Electrochem. Commun.*, 2003, **5**, 230.
217 W. C. West, N. V. Myung, J. F. Whitacre and B. V. Ratnakumar, *J. Power Sources*, 2004, **126**, 203.
218 J. J. Xu, G. Jain and J. Yang, *Electrochem. Solid-State Lett.*, 2002, **5**, A152.
219 J. J. Xu, J. Yang and G. Jain, *Electrochem. Solid-State Lett.*, 2002, **5**, A223.
220 J. S. Yang, T. B. Atwater and J. J. Xu, *J. Power Sources*, 2005, **139**, 274.
221 H. Furukawa, M. Hibino and I. J. Honma, *J. Electrochem. Soc.*, 2004, **151**, A527.
222 K. Lee and G. Z. Cao, *J. Phys. Chem. B*, 2005, **109**, 11880.
223 L. P. An, X. P. Gao, G. R. Li, T. Y. Yan, H. Y. Zhu and P. W. Shen, *Electrochim. Acta*, 2008, **53**, 4573.
224 S. W. Song and S. W. Baek, *Electrochem. Solid-State Lett.*, 2009, **12**, A23.
225 L. B. Chen, J. Y. Xie, H. C. Yu and T. H. Wang, *J. Appl. Electrochem.*, 2009, **39**, 1157.
226 V. Baranchugov, E. Markevich, E. Pollak, G. Salitra and D. Aurbach, *Electrochem. Commun.*, 2007, **9**, 796.
227 M. S. Park, G. X. Wang, H. K. Liu and S. X. Dou, *Electrochim. Acta*, 2006, **51**, 5246.
228 H. Xia, S. B. Tang and L. Lu, *Mater. Res. Bull.*, 2007, **42**, 1301.
229 T. J. Boyle, D. Ingersoll, T. M. Alam, C. J. Tafoya, M. A. Rodriguez, K. Vanheusden and D. H. Doughty, *Chem. Mater.*, 1998, **10**, 2270.
230 S. Gopukumar, K. Y. Chung and K. B. Kim, *Electrochim. Acta*, 2004, **49**, 803.
231 M. W. Raja, S. Mahanty and R. N. Basu, *J. Mater. Chem.*, 2009, **19**, 6161.
232 D. A. Totir, B. D. Cahan and D. A. Scherson, *Electrochim. Acta*, 1999, **45**, 161.
233 M. G. Lazarraga, S. Mandal, J. Ibanez, J. M. Amarilla and J. M. Rojo, *J. Power Sources*, 2003, **115**, 315.
234 E. P. Roth, D. H. Doughty and J. Franklin, *J. Power Sources*, 2004, **134**, 222.
235 M. Yoo, C. W. Frank, S. Mori and S. Yamaguchi, *Chem. Mater.*, 2004, **16**, 1945.
236 S. Ahn, *Electrochem. Solid-State Lett.*, 1999, **1**, 111.
237 X. M. Liu, Z. D. Huang, S. Oh, P. C. Ma, P. C. H. Chan, G. K. Vedam, K. Kang and J. K. Kim, *J. Power Sources*, 2010, **195**, 4290.
238 Y. J. Park, K. S. Ryu, K. M. Kim, N. G. Park, M. G. Kang and S. H. Chang, *Solid State Ionics*, 2002, **154–155**, 229.
239 H. K. Kim, T. Y. Seong and Y. S. Yoon, *Electrochem. Solid-State Lett.*, 2002, **5**, A252.
240 J. D. Perkins, C. S. Bahn, J. M. McGraw, P. A. Parilla and D. S. Ginley, *J. Electrochem. Soc.*, 2001, **148**, A1302.

241 N. Kuwata, J. Kawamura, K. Toribami, T. Hattori and N. Sata, *Electrochem. Commun.*, 2004, **6**, 417.
242 C. H. Chen, E. M. Kelder and J. Schoonman, *Thin Solid Films*, 1999, **342**, 35.
243 M. Mohamedi, M. Makino, K. Dokko, T. Itoh and I. Uchida, *Electrochim. Acta*, 2002, **48**, 79.
244 Y. J. Park, J. G. Kim, M. K. Kim, H. T. Chung and H. G. Kim, *Solid State Ionics*, 2000, **130**, 203.
245 Y. H. Rho, K. Kanamura and T. Umegaki, *J. Electrochem. Soc.*, 2003, **150**, A107.
246 M. Cheong and I. Zhitomirsky, *Surf. Eng.*, 2009, **25**, 346.
247 Y. H. Wang and I. Zhitomirsky, *Langmuir*, 2009, **25**, 9684.
248 Y. Wang and G. Z. Cao, *Electrochim. Acta*, 2006, **51**, 4865.
249 D. W. Liu, Q. F. Zhang, P. Xiao, B. B. Garcia, Q. Guo, R. Champion and G. Z. Cao, *Chem. Mater.*, 2008, **20**, 1376.
250 D. W. Liu, B. B. Garcia, Q. F. Zhang, Q. Guo, Y. H. Zhang, S. Sepehri and G. Z. Cao, *Adv. Funct. Mater*, 2009, **19**, 948.
251 S. M. Zhu, Z. Y. Zhou, D. Zhang and H. H. Wang, *Microporous Mesoporous Mater.*, 2006, **95**, 257.
252 C. Navone, J. P. Pereira-Ramos, R. Baddour-Hadjean and R. Salot, *J. Electrochem. Soc.*, 2006, **153**, A2287.
253 K. Le Van, H. Groult, A. Mantoux, L. Perrigaud, F. Lantelme, R. Lindstroem, R. Badour-Hadjean, S. Zanna and D. Lincot, *J. Power Sources*, 2006, **160**, 592.
254 L. Wang, H. W. Xu, P. C. Chen, D. W. Zhang, C. X. Ding and C. H. Chen, *J. Power Sources*, 2009, **193**, 846.
255 Y. Yu, J. L. Shui and C. H. Chen, *Solid State Commun.*, 2005, **135**, 485.
256 X. H. Huang, J. P. Tu, X. H. Xia, X. L. Wang, J. Y. Xiang, L. Zhang and Y. Zhou, *J. Power Sources*, 2009, **188**, 588.
257 P. Xiao, Y. H. Zhang, B. B. Garcia, S. Sepehri, D. W. Liu and G. Z. Cao, *J. Nanosci. Nanotechnol.*, 2009, **9**, 2426.
258 Y. H. Zhang, P. Xiao, X. Y. Zhou, D. W. Liu, B. B. Garcia and G. Z. Cao, *J. Mater. Chem.*, 2009, **19**, 948.